Earth and Planetary Science Letters 424 (2015) 95–108

Contents lists available at ScienceDirect

Earth and Planetary Science Letters

www.elsevier.com/locate/epsl

The Fish Canyon Tuff: A new look at an old low-temperature thermochronology standard

Andrew Gleadow [a,*], Mark Harrison [b], Barry Kohn [a], Rául Lugo-Zazueta [a,1], David Phillips [a]

[a] School of Earth Sciences, University of Melbourne, Victoria 3010, Australia
[b] Department of Earth, Planetary & Space Sciences, University of California, Los Angeles, CA 90095, USA

ARTICLE INFO

Article history:
Received 18 February 2015
Accepted 1 May 2015
Available online 27 May 2015
Editor: A. Yin

Keywords:
Fish Canyon Tuff
geochronology
thermochronology
age standard
(U–Th)/He
fission track

ABSTRACT

The Fish Canyon Tuff (FCT) has served as an important source for geochronology standards, particularly for fission track, K–Ar and (^{40}Ar/^{39}Ar) dating, even though efforts to establish precise ages for its constituent minerals have proved to be unexpectedly complex. To evaluate the suitability of FCT apatite as a standard for apatite (U–Th–Sm)/He (AHe) thermochronometry, and to test underlying assumptions about its suitability for apatite fission track (AFT) thermochronometry, we analysed samples from a series of sites throughout the vertical and lateral extent of the host ignimbrite sheet. Samples were collected from the relatively lithic-rich, classic sampling location in the lower part of the thick proximal ignimbrite and a ~330 m vertical section of FCT immediately above it. Average weighted mean AHe ages from multiple analyses at five sites in this profile range from 20.8 ± 0.4 Ma from the classic site at the base, to an average of 28.4 ± 0.2 Ma (all ±1σ) in the upper part of the section. The AHe age at the classic site is substantially reduced at 20.8 ± 0.4 Ma relative to a reference age for ignimbrite emplacement of 28.2 Ma. Corresponding zircon (U–Th)/He (ZHe) ages for these samples are all concordant at 28.3 ± 0.4 Ma. By contrast, apatite fission track (AFT) ages from the same vertical section are all concordant at 27.4 ± 0.7 Ma with the central age of 28.8 ± 0.8 Ma at the classic site, except for the uppermost sample (23.2 ± 1.7 Ma) for which clear evidence for local, probably fire, disturbance is seen in the track length distribution. The AHe data at the classic site thus provide evidence for substantial post-eruptive Early Miocene cooling of the tuff consistent with its position at the bottom of a deeply incised valley with ~800 m of local relief and probably >1000 m of removed section above it. The AFT age of the classic sampling site, however, is indistinguishable from ignimbrite emplacement and thus continues to be a useful standard for AFT (but not for AHe) geochronology. Apatites from this site have the highest measured Cl concentrations (0.82 wt%) of any of the FCT apatites analysed, contributing to this suitability. AFT and AHe ages at three distal localities, some 35–45 km to the East of the classic site, where the thickness of the FCT is reduced to <100 m, all yielded concordant ages with a weighted mean of 28.5 ± 0.11 Ma with no evidence for post-emplacement thermal disturbance. One of the distal sites – a quarry in the upper part of the FCT – appears to be an ideal locality for a standard reference material that would be suitable for both AFT and AHe low-temperature thermochronometers. U–Pb ages for zircons and ^{40}Ar/^{39}Ar step heating age spectra for sanidine at this new distal site are essentially identical to those found at the classic site.

1. Introduction

In principle, geochronologic methods based on radiogenic accumulation only require knowledge of the absolute abundances of parent and daughter products and the decay constant(s) (e.g., U–Th–Pb dating). In practice, however, certain of these approaches instead rely on mineral standards for which ages have been accurately determined by independent means. The reasons for this include poorly known decay constants (e.g., spontaneous fission of ^{238}U) and the need to characterise complex neutron energy spectra and capture cross sections during sample irradiation (e.g., fission track and ^{40}Ar/^{39}Ar dating; Mitchell, 1968; Hurford and Green, 1982). The use of basement rocks for this purpose is generally precluded by the variable retentivity of daughter isotopes across the spectrum of geochronometers coupled with protracted cooling.

* Corresponding author.
E-mail address: gleadow@unimelb.edu.au (A. Gleadow).
[1] Current address: Estación Regional del Noroeste, Instituto de Geología, Universidad Nacional Autónoma de México, 83240, Hermosillo, Sonora, México.

http://dx.doi.org/10.1016/j.epsl.2015.05.003
0012-821X/

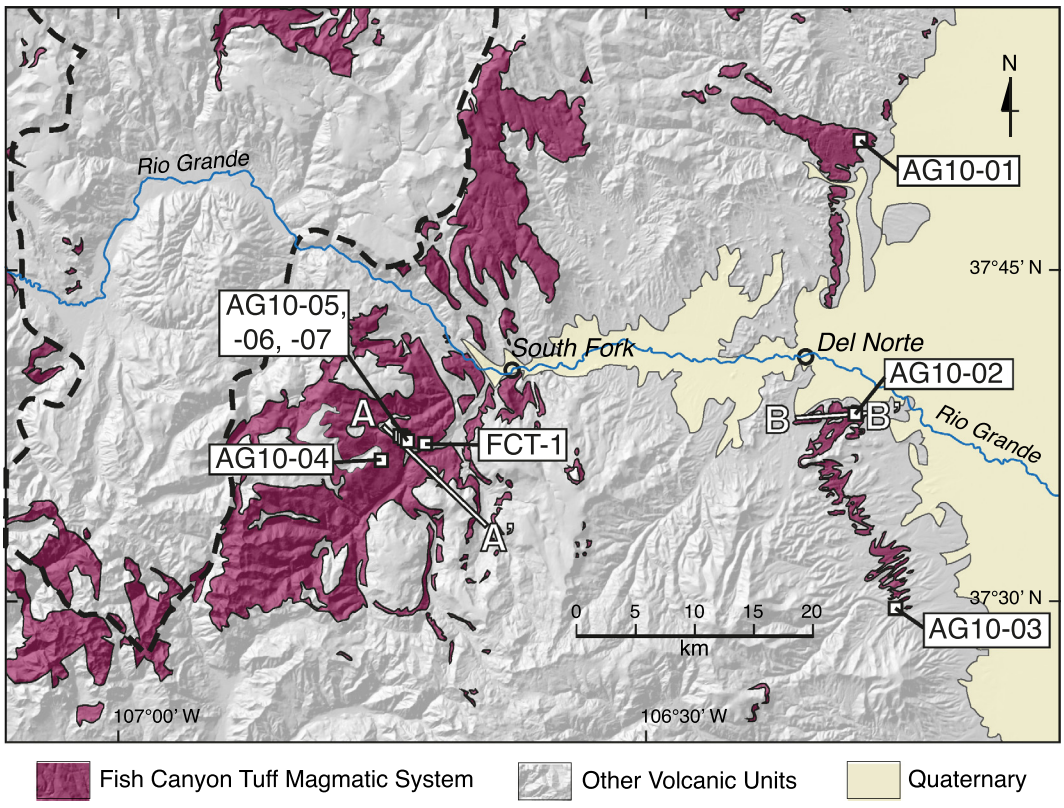

Fig. 1. Simplified geological map showing the distribution of the Fish Canyon Tuff based on the 1:250,000 geological map of Steven et al. (1974), and encompassing the later sub-divisions of the Fish Canyon magmatic system (Bachmann et al., 2007). The heavy dashed line shows the extent of the parent La Garita Caldera. Sample localities are also shown for both proximal and distal sites, and A–A', and B–B' show the two cross-sections in Fig. 2.

This limits candidate rocks to rapidly cooled, near-surface materials with simple and known thermal histories which contain a robust geochronometer whose age can be determined from first principles. Thus U–Pb dating of zircon from an undisturbed volcanic rock containing a host of commonly used geochronometers would appear to meet these requirements.

The Fish Canyon Tuff (FCT) is a voluminous crystal-rich ignimbrite sheet erupted over a relatively short period during the late Oligocene from the ca. 2500 km^2 La Garita Caldera in the San Juan volcanic field, southern Colorado (Lipman et al., 1970; Steven et al., 1974; Whitney and Stormer, 1985; Mason et al., 2004) (Fig. 1). The FCT appears to satisfy many of the criteria for an ideal dating standard material in that it has an excellent assemblage of dateable phenocryst and accessory minerals, the age of the rock makes it suitable for analysis by a wide spectrum of techniques, and the rock is readily accessible with an abundant supply of unaltered material. The dateable mineralogy includes plagioclase, sanidine, biotite, hornblende, titanite, apatite and zircon. For all of these minerals, the grainsize and freshness of the minerals is excellent. Steven et al. (1967) found an isochronous relationship at 27.9 ± 0.7 Ma (using the same decay constants and isotopic abundances as recommended by Steiger and Jäger, 1977) amongst the phenocryst phases in this rock dateable by the K–Ar method. This work laid the foundation for various minerals from the FCT being developed as age standards by a number of geochronology and thermochronology laboratories using a variety of mineral dating techniques.

Apatite and zircon from the Fish Canyon Tuff first came into widespread use in various fission track dating laboratories in the 1970s following its introduction by Chuck Naeser (Naeser et al., 1981). Subsequently, these and other minerals from this rock were investigated for use as inter- and intra-laboratory standards using the $^{40}Ar/^{39}Ar$, (U–Th–Sm)/He and U–Pb methods (Bachmann et al., 2000, 2002, 2007; Baksi et al., 1996; Carpena and Mailhé, 1987; Cebula et al., 1986; Daze et al., 2003; Dobson et al., 2008; Hurford and Hammerschmidt, 1985; Jourdan and Renne, 2007; Kuiper et al., 2008; Lanphere, 2004; Lanphere and Baadsgaard, 1997, 2001; Lanphere and Dalrymple, 2000; Lipman et al., 1970, 1997; Oberli et al., 1990, 2002; Reiners et al., 2002; Reiners and Farley, 1999; Renne, 1998; Renne et al., 1994, 1998, 2010, 2011; Schmitz and Bowring, 2001; Schmitz et al., 2003; Schwarz et al., 2010; Spell and McDougall, 2003; Tagami et al., 2003). A detailed review of these data is outside the purview of this paper, but for purposes of comparison we assume a reference age for ignimbrite emplacement of 28.2 Ma (Boehnke and Harrison, 2014).

Several concerns regarding this approach in general, and the use of the Fish Canyon Tuff in particular, subsequently arose. The recognition that zircons can crystallise and remain closed U–Pb systems in felsic magma chambers for up to half a million years prior to eruption (Reid et al., 1997) challenged the assumption of concordancy among all mineral dating systems. U–Pb zircon dating and thermal modelling (Bachmann and Bergantz, 2003; Bachmann et al., 2007; Wotzlaw et al., 2013) are consistent with the precursor FCT magma having existed as a crystal mush for over 400 ka in which zircons experienced protracted growth. Furthermore, the presence of abundant lithic clasts at the original sampling locality and its position at the base of a ca. 1000 m thick volcanic pile leaves open the possibility that this rock may contain mineral xenocrysts and did not effectively cool to ambient temperature instantaneously as required for an age standard, at least for the low-temperature systems.

In this paper we report new fission track and (U–Th–Sm)/He ages of apatites and zircons from a variety of sampling sites within the Fish Canyon Tuff, supported by comparative U–Pb zircon, and $^{40}Ar/^{39}Ar$ sanidine ages. Our sampling approach aimed to maximize opportunities to observe both vertical and lateral mineral age

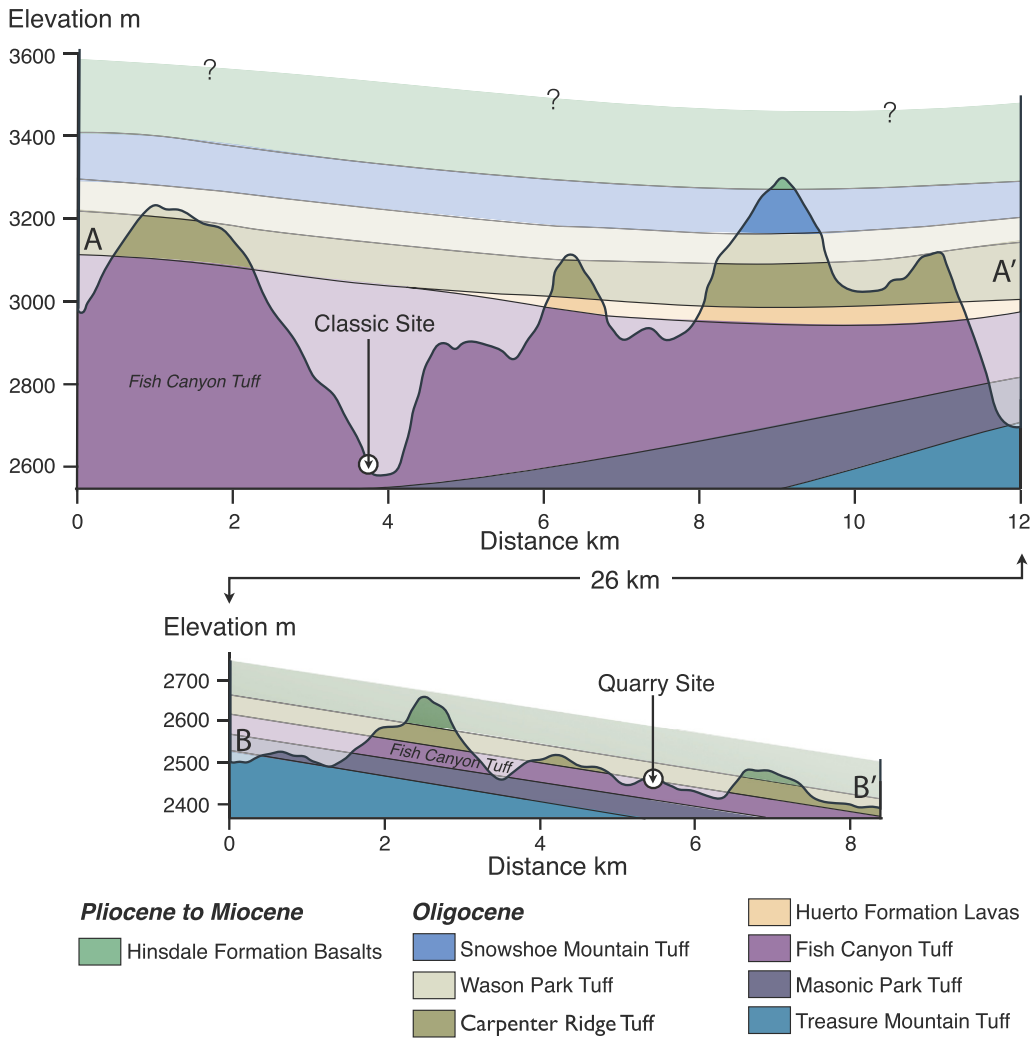

Fig. 2. Geological cross-sections through the volcanic pile based on the geological map of Steven et al. (1974). A–A' shows the proximal region including the classic sampling site for Fish Canyon Tuff age standards, and B–B' for the distal quarry location where the volcanic sequence is relatively condensed.

heterogeneities that may be present within the ignimbrite sheet, and particularly to compare the classic, proximal, site with distal sites where the thickness of the FCT diminishes to <100 m and the total cover was likely to never have exceeded ~150 m.

1.1. Geological considerations for an age standard

Compositionally the FCT is a crystal-rich biotite–hornblende–plagioclase quartz latite with minor quartz and sanidine (Lipman et al., 1970; Bachmann et al., 2002). Phenocryst phases are abundant and typically make up about 40% of the rock (Bachmann et al., 2000). The quarto-feldspathic groundmass hosts accessory apatite, zircon and titanite. The tuff is a typically densely welded and recrystallised ignimbrite erupted during the main collapse phase of the caldera (Lipman et al., 1970).

The classic sampling locality of Steven et al. (1967) (Fig. 1) is in a road cut on Colorado Highway 160 about 8.7 km southwest of the town of South Fork. The road has been realigned and rebuilt since the earliest use of this locality as a source of standard material in the 1970s, but now exposes even fresher and deeper road cuts than available previously. The presently available sampling site is no more than a few tens of metres at most from the original site.

The classic site lies at the bottom of a deep valley with local relief to the nearby peaks of over 800 m and a total thickness of removed overlying section that probably exceeds 1000 m. The FCT is overlain in turn by several other substantial volcanic units of Oligocene and younger age (Steven et al., 1974). The sample site itself is near the bottom of the major FCT ignimbrite sheet, which is more than 600 m thick at this proximal locality about 15 km from the edge of the La Garita Caldera, as shown in the cross section (Fig. 2) produced by draping the mapped geological units (Steven et al., 1974) over the digital topography. The depth of erosion at this site thus appears far from ideal for capturing concordancy between high and low-temperature thermochronologic systems and yet this aspect of the site's suitability has not previously been tested.

As shown in Fig. 2a, the classic sampling locality appears to have been exhumed from a depth of >1000 m below the post-volcanic land surface and only became exposed at the surface following substantial later erosion. Such an erosional depth opens the possibility that post-emplacement temperatures were high enough to disturb at least the apatite (U–Th)/He system. There was also a suggestion in a number of early fission track measurements that the apatite FT age may be lower than independent $^{40}Ar/^{39}Ar$ reference ages (Naeser et al., 1981). These discrepancies were thought at the time to largely reflect problems in system calibration that were resolved by general adoption of an empirical calibration against an agreed set of age standards (i.e., zeta-calibration; Hurford and Green, 1982). However as the FCT was one of the

Table 1
Fish Canyon Tuff – sample location data.

Sample No.	Latitude	Longitude	Elevation (m)	Locality	Flow section	Lithic clasts
Distal sites:						
AG10-01	37°50'52.56"N	106°16'32.04"W	2418	Roadcut, 19.75 kn NNE of Del Norte, Co	Distal Location	Lithic rich
AG10-02	37°38'22.44"N	106°17'57.90"W	2467	Quarry, 6 km SE of Del Norte	Distal Location	Lithic poor
AG10-03	37°29'27.74"N	106°15'39.23"W	2543	Rock Creek, 13 km SW of Monte Vista	Distal Location	Lithic rich
Proximal section:						
AG10-04	37°37'04.56"N	106°43'41.10"W	2913	Outcrop beside minor road above FCT-1 site	Proximal Section	Lithic poor
AG10-05	37°37'22.08"N	106°43'02.70"W	2856	Roadcut above FCT-1 site	Proximal Section	Lithic rich
AG10-06	37°37'18.24"N	106°42'56.82"W	2847	Roadcut above FCT-1 site	Proximal Section	Lithic free
AG10-07	37°37'13.44"N	106°42'46.86"W	2831	Roadcut above FCT-1 site	Proximal Section	Lithic rich
Classic site:						
FCT-1	37°36'40.27"N	106°42'19.84"W	2580	Classic Site, road cut, 8.7 km SW of South Fork	Proximal Section	Lithic rich

most important and widely adopted age standards in this process, a lingering concern remained that a systematic error in FT age calibration could have been introduced.

Foremost amongst the requirements for an age standard that can serve the needs of both high-temperature and low-temperature thermochronometry systems is that the constituent minerals formed simultaneously, cooled rapidly at the time of eruption, and subsequently remained at near-surface conditions. The geological setting of the classic FCT sampling location shows that the latter conditions are unlikely to have been met for the lowest temperature systems, especially apatite (U–Th)/He (AHe), and conceivably also apatite fission track analysis (AFT).

For high-temperature systems, such as zircon U–Pb, the high proportion of lithic clasts at the classic site also raises some questions about possible inheritance of older grains from the clast source. In addition there is the aforementioned possibility of inheritance from pre-eruption crystallisation in the magma chamber (Reid et al., 1997).

The valley sides at the classic locality show a series of cliff forming horizons within the single FCT cooling unit, suggesting it consists of a several individual flow units in this area that cooled and partially recrystallised as a single cooling unit in this area. Lithic clasts mostly consist of fine- to medium-grained silicic volcanic rocks and appear to be concentrated close to the bottom of these individual flow units. The clasts are typically up to about 3 cm across and occur in an abundance of approximately 50 per square metre on a planar surface at this locality, and also at other localities that were sampled near the base of individual flow units. The upper flow units are relatively free from clasts, providing an opportunity to test their possible influence on the different radiometric systems.

1.2. Sampling strategy

The primary intent of our sampling was to fully test possible limitations of the classic sampling locality and to examine the possibility that more suitable material might be found at another locality that better meets the needs of a reference material for both high-temperature and low-temperature systems. Specifically, examination of fission track and (U–Th)/He ages of apatites at distal locations of the Fish Canyon Tuff ignimbrite sheet where the total thickness of both the FCT itself and all overlying units are sufficiently thin (<200 m) better assures an essentially surface-like post-emplacement temperature history and provides a baseline with which to compare results from the classic locality. Sampling the vertical section above the classic site for AFT and AHe dating permits a second approach to test possible complications for the low-temperature systems at this locality by sampling rocks that were closer to the pre-erosion, post-volcanic land surface. Lastly, we obtained samples containing varying abundances of lithic inclusions with the view to examining a possible relationship between lithic content and the presence of xenocrystic zircon.

1.3. Proximal samples

We returned as closely as is now possible to the classic sampling site and sampled the lithic-rich tuff (Fig. 1), hereinafter referred to as FCT-1. We then sampled a vertical section of FCT above that site along a switchback track (samples AG10-04 to AG10-07) that provided ~330 m relief, albeit with all samples coming from the upper ~100 m of the traverse (thus enhancing the potential to reveal vertical contrasts). Samples AG10-04 and AG10-06 are from the upper parts of individual flow units within the overall FCT cooling unit and are lithic-poor, whereas AG10-05 and AG10-07 are lithic-rich (Table 1).

1.4. Distal samples

We sampled several distal localities, some 35–45 km to the NE, E and ESE of the classic site, where the FCT displays a total thickness of only a few tens of meters (Figs. 2b, c). Sample AG10-01 was obtained from a roadcut ~20 km NNE of Del Norte (Fig. 1). The FCT thickness at this locality appears somewhat greater at ~100 m than for other distal sites. The rock is a crystal- and lithic-rich tuff with feldspar, quartz and biotite grains supported in a fine-grained groundmass.

Sample AG10-02, from a quarry 4.6 km SE of Del Norte and about 1.8 km west of Route 160, is a pale, crystal-rich ignimbrite (Fig. 1). This quarry is the easternmost of several excavated pits up to 40 × 20 m in size, and readily accessible by a small track from Route 160. This quarry appears to be the source of building stone for many of the masonry structures in the nearby towns. The FCT at this site is only ~40 m thick and part of a layered volcanic sequence dipping at 1–2° to the east where all of the units are condensed relative to their much greater thickness in the proximal region. From Fig. 2 it can be seen that the total thickness of the overlying volcanic pile at this locality is likely to be <150 m. Moreover, only rare (~5/m^2) cm-sized lithic clasts are present, consistent with the quarry being near the top of the flow. The extensive and relatively recent quarrying at this location provides access to abundant fresh sample material. The rock at this locality shows a pale pinkish-brown colour but in all other respects is essentially identical in mineralogy and texture to the grey rock at the classic site.

Sample AG10-03 was collected ~13 km SW of Monte Vista (Fig. 1) from a freshly fallen block at the base of a ~30 m high cliff developed in the FCT on the northeast bank of Rock Creek. This sample, a moderately welded crystal- and lithic-rich rhyolitic ignimbrite, represents the most distant from the inferred centre of the La Garita caldera (Steven et al., 1974).

Table 2
Fish Canyon Tuff zircon U–Pb data.

Sample/spot	*U* (ppm)	Th (ppm)	$^{238}U/^{206}Pb$	$^{238}U/^{206}Pb \pm 1$ s.e.	% $^{206}Pb^*$	$^{207}Pb^*/^{206}Pb^*$	$^{207}Pb^*/^{206}Pb^* \pm 1$ s.e.	$^{238}U/^{206}Pb$ age (Ma)	$\pm 1\sigma$ (Ma)
Rims									
FCT-1@1	442	162	210.9	5.6	99.4	0.0511	0.0023	30.4	0.8
FCT-1@1B	667	308	220.8	7.3	98.4	0.0594	0.0020	28.7	1.0
FCT-1@2	305	103	207.1	6.6	98.9	0.0552	0.0043	30.8	1.0
FCT-1@3	858	397	206.5	6.6	99.2	0.0525	0.0014	31.0	1.0
FCT-1@4	309	105	211.9	6.5	98.5	0.0581	0.0030	30.0	0.9
FCT-1@4B	348	160	216.8	6.7	98.8	0.0564	0.0027	29.4	0.9
FCT-1@5	440	187	211.6	7.3	99.2	0.0532	0.0030	30.2	1.1
FCT-1@5B	423	187	228.8	6.3	99.1	0.0538	0.0022	27.9	0.8
FCT-1@6	347	187	227.4	8.6	95.8	0.0795	0.0073	27.2	1.1
FCT-1@7	478	206	23.0	2.7	9.4	0.7545	0.0099	26.5	45.7
Weighted mean age 29.5 ± 0.3 *Ma (MSWD* = 1.7; *n* = 7)									
Interiors									
FCT-1p@1	297	144	225.1	5.2	99.9	0.0470	0.0026	28.6	0.7
FCT-1p@2	620	245	227.9	5.8	99.8	0.0481	0.0016	28.3	0.7
FCT-1p@3	444	160	216.8	5.2	99.7	0.0492	0.0019	29.7	0.7
FCT-1p@4	235	61	183.9	11.6	81.0	0.1951	0.0279	28.4	2.7
FCT-1p@5	292	69	218.8	5.3	100.0	0.0463	0.0029	29.5	0.7
FCT-1p@6	312	199	216.3	5.5	99.4	0.0512	0.0026	29.6	0.8
FCT-1p@7	76	17	237.2	8.5	99.3	0.0519	0.0066	27.0	1.0
FCT-1p@8	103	30	228.9	8.0	98.7	0.0564	0.0048	27.8	1.0
FCT-1p@9	854	245	216.8	4.7	100.0	0.0463	0.0014	29.8	0.6
FCT-1p@10	106	43	217.0	6.7	99.2	0.0528	0.0044	29.5	0.9
Weighted mean age 29.0 ± 0.3 *Ma (MSWD* = 1.2; *n* = 10)									
Rims									
AG10_02@1	473	204	220.8	6.5	99.8	0.0482	0.0021	29.2	0.9
AG10_02@1B	539	247	247.6	6.7	100.3	0.0444	0.0023	26.1	0.7
AG10_02@2	479	209	197.8	6.4	99.6	0.0500	0.0022	32.5	1.1
AG10_02@2B	492	217	164.4	6.7	99.3	0.0520	0.0026	38.9	1.6
AG10_02@3	451	237	218.0	6.8	95.1	0.0846	0.0037	28.2	0.9
AG10_02@3B	452	192	186.6	4.8	96.4	0.0746	0.0024	33.3	0.9
AG10_02@4	494	246	218.3	6.8	95.2	0.0842	0.0064	28.1	1.0
AG10_02@5	455	198	232.6	7.8	99.3	0.0518	0.0027	27.6	0.9
AG10_02@5B	515	235	254.8	7.5	96.1	0.0769	0.0089	24.4	0.8
AG10_02@6	439	192	211.2	5.4	97.8	0.0636	0.0036	29.9	0.8
Weighted mean age 28.5 ± 0.3 *Ma (MSWD* = 11; *n* = 6)									
Interiors									
AG10_02p@1	535	183	220.7	5.6	99.2	0.0525	0.0022	29.0	0.7
AG10_02p@2	461	163	224.1	4.9	99.6	0.0498	0.0021	28.7	0.6
AG10_02p@3	568	194	213.9	4.8	100.1	0.0458	0.0019	30.2	0.7
AG10_02p@4	398	178	219.9	6.2	99.4	0.0509	0.0028	29.2	0.8
AG10_02p@5	555	210	221.2	4.9	99.7	0.0487	0.0020	29.1	0.6
AG10_02p@6	632	244	225.3	5.0	99.8	0.0484	0.0017	28.6	0.6
AG10_02p@7	420	135	231.2	5.4	99.6	0.0494	0.0022	27.8	0.7
AG10_02p@8	797	348	213.5	5.1	99.8	0.0484	0.0015	30.1	0.7
AG10_02p@9	373	94	223.4	5.6	99.9	0.0475	0.0022	28.8	0.7
Weighted mean age 29.0 ± 0.2 *Ma (MSWD* = 12; *n* = 9)									

2. Analytical methods

2.1. Sample preparation

All samples were crushed in two stages using a jaw crusher and plate mill, then passed over a *Gemini* shaking table under flowing water to concentrate light and heavy components and remove fines. The resulting fractions were then dried and separated into constituent minerals using standard heavy liquid (sodium polytungstate and methylene iodide) and magnetic techniques. Final heavy concentrates were centrifuged in small volume tubes with Methylene Iodide to enhance the separation of apatite and zircon. Sanidines were hand picked from heavy liquid feldspar concentrates.

2.2. Ion microprobe analysis

Ion microprobe U–Pb zircon dating methods are described in Quidelleur et al. (1997) with the exception of those samples that were first pressed flush into indium metal and analysed unpolished to permit the last crystallised zircon layers to be dated by depth profiling. The epoxy mounts were then ground and polished down ~20 μm and re-analysed for U–Pb (designated 'p' in Table 2). Calculated ages were based on concurrent analysis of AS3 zircon standard (U–Pb age = 1099.1 ± 0.5 Ma; Paces and Miller, 1993) which reproduced during the ion microprobe session at the ±1% level. U–Pb zircon analytical data are given in Table 2.

2.3. $^{40}Ar/^{39}Ar$ analysis

Hand-picked sanidine crystals from sample AG10-02 were ultrasonically cleaned in 3% HF and washed with di-ionised water and acetone. Approximately 60 grains of AG10-02 were co-irradiated in the Cd-shielded CLICIT facility of the Oregon State University TRIGA reactor (can UM#52), together with Fish Canyon sanidine grains from the classic site. Fusion and step-heating analyses were carried out using a Thermo Fisher Scientific ARGUS VI multi-collector noble gas mass spectrometer (see detailed descriptions by Phillips and Matchan, 2013 and Matchan and Phillips, 2014). Sample heating was carried out using a homogenised 55 W Fusions 10.6 CO_2 laser system to achieve uniform heating over the sanidine crystals.

Results are shown in Table 3 and the step heating $^{40}Ar/^{39}Ar$ age spectra together with the mean single grain fusion age in Fig. 3.

Argon isotopic results are corrected for system blanks, mass discrimination, radioactive decay and reactor-induced interference reactions are given in Table 3. Line blanks were measured after every second or third sample analysis and were typically <1.5 fA for ^{40}Ar, compared to ≥ 100 fA for typical sample analyses. Mass discrimination and detector bias were characterised via automated analyses of air pipette aliquots prior to the first analysis, assuming an atmospheric $^{40}Ar/^{36}Ar$ ratio of 298.56 ± 0.31 (Lee et al., 2006). Interference correction factors determined for K-glass and Ca-salts were: $(^{39}Ar/^{37}Ar)_{Ca} = (6.5075 \pm 0.0033) \times 10^{-4}$; $(^{36}Ar/^{37}Ar)_{Ca} = (2.5680 \pm 0.0017) \times 10^{-4}$; $(^{40}Ar/^{39}Ar)_{K} = (5.93 \pm 0.18) \times 10^{-4}$; and $(^{38}Ar/^{39}Ar)_{K} = (1.20550 \pm 0.00072) \times 10^{-2}$. Apparent ages are calculated relative to an age of 28.20 Ma for the Fish Canyon Tuff sanidine, using the decay constants of Steiger and Jäger (1977). Unless otherwise stated, uncertainties are reported at the 1σ level for consistency with the other methods used here.

2.4. (U–Th–Sm)/He analysis

Analysis followed the protocol of House et al. (2000) for laser He extraction from single grains for both apatite and zircon. Clear, non-fractured euhedral grains with average grain radii in a close size range were hand picked under an Olympus SZX12 binocular microscope, then immersed in ethanol and checked under polarised light to detect and exclude grains with possible inclusions. Grain geometries were imaged microscopically, measured and stored for applying the α-ejection correction (Farley et al., 1996) and then loaded into small, acid-treated platinum capsules.

Apatite grains were outgassed under vacuum at ~900 °C for 5 min, using a Coherent Quattro FAP 820 nm diode laser, with a fibre-optic coupling to the sample chamber. He content was determined by isotope dilution using a pure ^{3}He spike, calibrated against an independent ^{4}He standard and measured using a Balzers quadrupole (Prisma QMS 200) mass spectrometer. Zircons were outgassed using a laser power of ~12.6 W (~1300 °C) applied for 20 min to ensure complete extraction of ^{4}He. A hot blank was run after each extraction to verify complete outgassing. All He extractions were performed on single grains except for three of the FCT-1 apatite measurements, which used aliquots of three grains.

Outgassed grains were removed from the laser chamber, dissolved and analysed for parent isotopes using an Agilent 7700X ICP Mass Spectrometer. Zircon grains were removed from their Pt capsules, and transferred to Parr bombs where they were spiked with ^{235}U and ^{230}Th and digested in small volumes (0.3–0.5 ml) at 240 °C for 40 h in HF. Standard solutions containing the same spike amounts as samples were treated identically, as were a series of unspiked reagent blanks. A second bombing in HCl for 24 h at 200 °C ensured dissolution of fluoride salts. Zircon solutions were then dried down, dissolved in HNO_3 and diluted in H_2O to 5% acidity for analysis of ^{238}U, ^{235}U, and ^{232}Th by solution ICP-MS. U and Th isotope ratios were measured to a precision of <2% and overall precision for the zircon (U–Th)/He ages is estimated at ~6% or less. Zircon He ages were calculated and corrected for α-emission following the approach of Hourigan et al. (2005). Zircon (U–Th)/He analytical data are shown in Table 4.

Apatites were dissolved (still in their Pt capsules) in HNO_3 and analysed for ^{238}U, ^{235}U, ^{232}Th and ^{147}Sm. Analyses were calibrated using the reference material BHVO-1, with Mud Tank Carbonatite apatite, and international rock standard BCR-2 used as check standards with each batch of samples analysed. (U–Th–Sm)/He ages were calculated and corrected for α-emission following the approach of Farley et al. (1996). Analytical uncertainties for the Melbourne He facility are conservatively assessed to be ~6.2%, including the α-ejection correction, an estimated 5 µm uncertainty in grain dimensions, gas analysis (estimated as <1%) and ICP-MS analytical uncertainties, but not possible heterogeneity in U and Th distributions. Accuracy and precision of U, Th and Sm content ranges up to 2%, but is typically better than 1%. Durango apatite was also run as an 'unknown' with each batch of samples and served as a check on sample accuracy. Apatite (U–Th–Sm)/He data are given in Table 5.

2.5. Fission track analysis

Fission track analysis of separated apatites was carried out using a new integrated analytical system based on autonomous digital microscopy for the capture of comprehensive fission track image sets, coupled with direct ^{238}U determination by laser-ablation ICP-MS. The analytical methods used for this new approach are given in greater detail in Appendix A. Two apatite grain mounts were prepared for each sample using epoxy on glass slides, polishing with diamond pastes on a *Struers* Rotopol automated polishing machine (to a 1 µm finish), and etched in 5N HNO_3 at 20 °C for 20 s.

Fission tracks were counted automatically on multi-plane digital images captured in reflected and transmitted light at 1000× magnification on a Zeiss M1m Axio-Imager microscope operating under *Autoscan TrackWorks* control software. Approximately 40 grains were selected for counting in each mount from an automatically ranked list determined from a scan of the whole mount under circular polarised light. Spontaneous tracks were counted automatically on the captured image sets using *FastTracks* image analysis software and manually corrected where necessary (Gleadow et al., 2009). Suitable confined tracks were identified and imaged on the second mount after ^{252}Cf irradiation to enhance the yield of suitable tracks (Donelick and Miller, 1991). The true lengths (dip corrected) were then measured for tracks with shallow dips ranging up to 20° using *FastTracks*. The resulting lengths are more precise, but comparable to conventional 'horizontal' confined track measurements.

After counting, the ^{238}U concentrations were determined on the same grains by laser-ablation ICP-MS, using a New Wave UP213 Laser microprobe and an Agilent 7700X ICP Mass Spectrometer. A laser pulse rate of 5 Hz, spot size of 30 µm, and power setting of 45% were used, and ablation was carried out under He then transported into the plasma using Ar carrier gas. ^{43}Ca was used as an internal standard in the apatites and the $^{238}U/^{43}Ca$ ratio measured against NIST612 glasses and Mud Tank and Durango apatite matrix-matched standards. Three to four ablation pits were ablated to a depth of ~8 µm on each grain with generally excellent agreement between the repeat analyses.

Fission Track ages were calculated from the spontaneous track densities and single grain ^{238}U concentrations as described by Hasebe et al. (2004) using an aggregate constant of 2.010×10^{-3}, equivalent to the zeta constant in the conventional External Detector Method, as discussed in Appendix A. Central ages and radial plots were calculated using the *RadialPlotter* package of Vermeesch (2009).

Apatite fission track results for all of the FCT samples are given in Table 6, a combined radial plot for the single grain data for all samples (except AG10-04, see below) in Fig. 4a, and confined track length distribution for the same apatite samples in Fig. 4b.

3. Results and discussion

U–Pb dating of zircons from both the classic sampling location (FCT-1) and the distal quarry site (AG10-02) were undertaken by ion microprobe to investigate protracted crystallisation histories and possible xenocrystic contamination between lithic-rich and lithic-poor samples. To maximize the temporal resolu-

Table 3
Fish Canyon Tuff AG10-02 sanidine $^{40}Ar/^{39}Ar$ results.

Sample ID	Step No.	Laser power (W)	^{40}Ar (fA)	$\pm1\sigma$	^{39}Ar (fA)	$\pm1\sigma$	^{38}Ar (fA)	$\pm1\sigma$	^{37}Ar (fA)	$\pm1\sigma$	^{36}Ar (fA)	$\pm1\sigma$	^{39}Ar ($\times10^{-14}$ mol)[b]	Ca/K	±	%^{40}Ar*	$^{40}Ar^*/^{39}Ar$	$\pm1\sigma$	Cum. %^{39}Ar	Apparent age (Ma)	$\pm1\sigma$ (Ma)
Sample AG10-02A (single-grain laser fusion results)																					
AG10-02-1	1	8.47	1799.24	0.56	2790.65	0.92	0.02258	0.00013	24.54	0.11	0.1198	0.0007	9.9068	0.01539	0.00007	97.92	0.63193	0.00030	13.25	28.189	0.013
AG10-02-2	1	8.47	1492.87	0.43	2284.21	0.75	0.03175	0.00019	22.25	0.06	0.1684	0.0010	8.1089	0.01705	0.00005	96.54	0.63154	0.00031	24.09	28.172	0.014
AG10-02-3	1	8.47	1676.74	0.57	2591.36	0.86	0.02468	0.00016	19.38	0.06	0.1309	0.0008	9.1993	0.01309	0.00004	97.58	0.63196	0.00032	36.39	28.190	0.014
AG10-02-4	1	8.47	1575.39	0.40	2472.94	0.64	0.00850	0.00012	21.07	0.07	0.0451	0.0006	8.7789	0.01491	0.00005	99.05	0.63161	0.00024	48.13	28.175	0.011
AG10-02-5	1	8.47	1411.48	0.92	2227.49	1.34	0.00273	0.00012	22.33	0.11	0.0145	0.0007	7.9076	0.01754	0.00009	99.60	0.63172	0.00057	58.71	28.180	0.025
AG10-02-6	1	8.47	1062.44	0.38	1675.33	0.60	0.00240	0.00014	12.48	0.09	0.0127	0.0007	5.9474	0.01303	0.00009	99.55	0.63190	0.00035	66.66	28.188	0.015
AG10-02-7	1	8.47	1224.56	0.41	1923.55	0.67	0.00589	0.00009	15.37	0.10	0.0313	0.0005	6.8286	0.01398	0.00009	99.15	0.63177	0.00031	75.79	28.182	0.014
AG10-02-8	1	8.47	1577.83	0.51	2466.29	0.79	0.01242	0.00014	23.34	0.16	0.0659	0.0007	8.7553	0.01656	0.00011	98.66	0.63178	0.00030	87.50	28.182	0.013
AG10-02-10	1	8.47	1127.84	0.41	1775.08	0.60	0.00369	0.00013	12.28	0.08	0.0196	0.0007	6.3015	0.01211	0.00008	99.39	0.63208	0.00033	95.93	28.196	0.015
AG10-02-11	1	8.47	550.39	0.15	857.50	0.27	0.00502	0.00022	191.02	0.12	0.0267	0.0012	3.0441	0.38984	0.00028	98.46	0.63257	0.00048	100.00	28.217	0.021
																				Weighted mean age ($n = 10$): 28.185 ± 0.012 Ma (2σ)	
Sample AG10-02B (step-heating experiment, 25 grains)																					
AG10-02-B1	1	0.77	1310.58	0.42	2057.35	0.66	0.00864	0.00016	15.10	0.09	0.0458	0.0008	7.3036	0.01284	0.00008	98.86	0.63037	0.00031	20.43	28.120	0.014
AG10-02-B2	2	0.82	1139.98	0.40	1789.86	0.68	0.00700	0.00010	12.85	0.07	0.0371	0.0005	6.3540	0.01256	0.00007	98.94	0.63072	0.00034	38.21	28.135	0.015
AG10-02-B3	3	0.88	1038.61	0.29	1637.12	0.52	0.00303	0.00010	11.72	0.13	0.0161	0.0006	5.8118	0.01253	0.00014	99.44	0.63148	0.00029	54.47	28.169	0.013
AG10-02-B4	4	0.93	858.59	0.22	1353.00	0.43	0.00215	0.00012	9.83	0.13	0.0114	0.0006	4.8031	0.01271	0.00017	99.51	0.63207	0.00030	67.91	28.195	0.013
AG10-02-B5	5	1.07	473.78	0.16	746.39	0.28	0.00096	0.00005	5.17	0.07	0.0051	0.0002	2.6497	0.01213	0.00017	99.59	0.63273	0.00033	75.32	28.224	0.015
AG10-02-B6	6	1.18	410.05	0.15	645.48	0.26	0.00053	0.00007	4.73	0.06	0.0028	0.0004	2.2914	0.01284	0.00016	99.70	0.63396	0.00039	81.73	28.279	0.017
AG10-02-B7	7	1.33	285.69	0.11	449.94	0.13	0.00039	0.00005	3.02	0.09	0.0021	0.0003	1.5973	0.01174	0.00034	99.69	0.63359	0.00037	86.20	28.262	0.016
AG10-02-B8	8	1.61	226.67	0.08	356.33	0.14	0.00021	0.00006	2.44	0.10	0.0011	0.0003	1.2650	0.01197	0.00048	99.76	0.63518	0.00042	89.74	28.333	0.019
AG10-02-B9	9	2.52	365.43	0.15	572.95	0.21	0.00055	0.00005	4.05	0.07	0.0029	0.0003	2.0340	0.01236	0.00023	99.67	0.63628	0.00038	95.43	28.381	0.017
AG10-02-B10	10	8.47	294.74	0.09	459.86	0.18	0.00056	0.00009	3.20	0.11	0.0030	0.0005	1.6325	0.01217	0.00042	99.61	0.63902	0.00045	100.00	28.503	0.020
																				Total gas age = 28.205 ± 0.030 Ma (2σ)	
Sample AG10-02C (step-heating experiment, 20 grains)																					
AG10-02-C1	1	0.25	25.85	0.02	19.81	0.02	0.00802	0.00012	0.36	0.14	0.0425	0.0006	0.0703	0.03187	0.01263	50.86	0.66417	0.00949	0.24	29.615	0.420
AG10-02-C2	2	0.38	65.46	0.03	86.62	0.03	0.00587	0.00008	1.29	0.11	0.0311	0.0004	0.3075	0.02612	0.00218	85.74	0.64847	0.00144	1.28	28.921	0.064
AG10-02-C3	3	0.51	162.44	0.04	245.30	0.08	0.00467	0.00009	2.19	0.17	0.0248	0.0005	0.8708	0.01560	0.00122	95.36	0.63208	0.00061	4.23	28.196	0.027
AG10-02-C4	4	0.63	488.99	0.13	760.77	0.24	0.00626	0.00009	6.58	0.28	0.0332	0.0005	2.7007	0.01515	0.00064	97.88	0.62972	0.00032	13.37	28.091	0.014
AG10-02-C5	5	0.76	814.23	0.25	1279.31	0.41	0.00563	0.00007	9.82	0.31	0.0298	0.0004	4.5415	0.01344	0.00043	98.81	0.62950	0.00029	28.74	28.081	0.013
AG10-02-C6	6	0.88	635.99	0.19	1000.84	0.36	0.00296	0.00012	7.60	0.28	0.0157	0.0006	3.5530	0.01329	0.00048	99.17	0.63077	0.00035	40.77	28.137	0.015
AG10-02-C7	7	1.00	873.39	0.25	1375.03	0.45	0.00341	0.00012	10.99	0.28	0.0181	0.0006	4.8814	0.01399	0.00036	99.29	0.63126	0.00031	57.30	28.159	0.014
AG10-02-C8	8	1.11	573.46	0.20	901.78	0.32	0.00227	0.00010	6.82	0.26	0.0121	0.0005	3.2013	0.01324	0.00050	99.28	0.63193	0.00036	68.13	28.189	0.016
AG10-02-C9	9	1.22	246.32	0.08	387.25	0.09	0.00086	0.00008	2.79	0.26	0.0046	0.0004	1.3747	0.01263	0.00117	99.36	0.63255	0.00042	72.79	28.216	0.019
AG10-02-C10	10	1.44	180.43	0.07	282.99	0.09	0.00059	0.00004	1.96	0.20	0.0032	0.0002	1.0046	0.01215	0.00124	99.39	0.63426	0.00042	76.19	28.292	0.018
AG10-02-C11	11	4.20	774.51	0.19	1214.96	0.38	0.00391	0.00005	9.44	0.24	0.0207	0.0003	4.3131	0.01359	0.00035	99.11	0.63238	0.00026	90.79	28.209	0.012
AG10-02-C12	12	8.47	412.18	0.14	631.64	0.21	0.00611	0.00013	5.19	0.20	0.0324	0.0007	2.2423	0.01437	0.00057	97.57	0.63724	0.00046	98.38	28.424	0.020
AG10-02-C13	13	9.40	94.79	0.03	134.68	0.05	0.00530	0.00017	1.17	0.20	0.0281	0.0009	0.4781	0.01515	0.00263	91.06	0.64147	0.00201	100.00	28.611	0.089
																				Total gas age = 28.196 ± 0.030 Ma (2σ)	

[a] Data are corrected for mass spectrometer backgrounds, discrimination, radioactive decay and neutron-induced interferences. Errors are one sigma uncertainties and exclude uncertainties in the J-value. The air argon isotopic ratio of Lee et al. (2006) is assumed.

[b] ^{39}Ar mole intensities (corrected for mass spectrometer backgrounds, discrimination and radioactive decay) calculated assuming a sensitivity value of 3.55×10^{-17} mol/mA.

[c] Interference correction values are: $(^{39}Ar/^{37}Ar)_{Ca} = (6.5075 \pm 0.0033) \times 10^{-4}$; $(^{36}Ar/^{37}Ar)_{Ca} = (2.5680 \pm 0.0017) \times 10^{-4}$; $(^{40}Ar/^{39}Ar)_{K} = (5.93 \pm 0.16) \times 10^{-4}$; and $(^{38}Ar/^{39}Ar)_{K} = (1.20550 \pm 0.00072) \times 10^{-2}$. Apparent ages are calculated using a J-value of 0.0249202± 0.0000034 (1σ), based on an age of 28.20 Ma for Fish Canyon Tuff sanidine.

[d] Line blank values are corrected for mass discrimination.

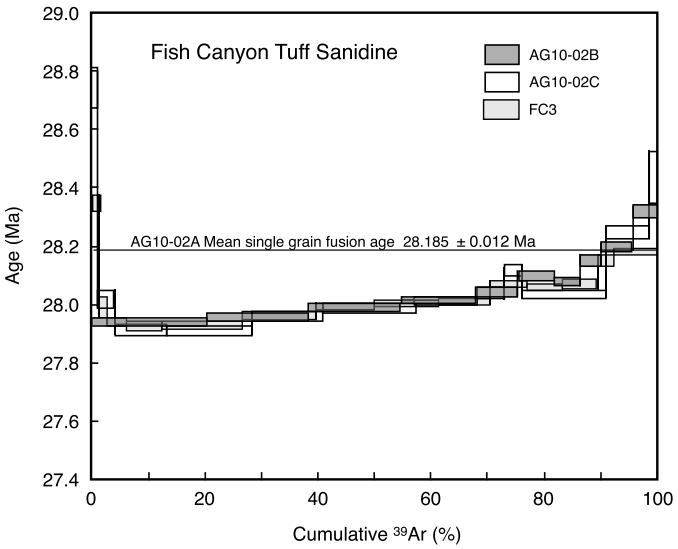

Fig. 3. ^{40}Ar/^{39}Ar step-heating spectra for two aliquots of grains from Fish Canyon Tuff sanidine from AG10-02 (B and C) from the distal quarry site, compared to sample FC3 sanidine from the classic site (from Phillips and Matchan, 2013). These three release spectra are essentially identical. For comparison, the mean of ten single grain fusion ages for AG10-02 is also shown as a horizontal line.

tion of the approach, we examined both zircon rims and cores. Weighted mean averages of FCT-1 rim and FCT-1 core yielded indistinguishable ages of 29.3 ± 0.3 Ma (all 1σ) (*MSWD* = 1.7) and 29.0 ± 0.3 Ma (1σ) (*MSWD* = 1.2), respectively. The polished AG10-02 weighted mean age of 29.0 ± 0.2 Ma (*MSWD* = 1.2) is statistically identical to the FCT-1 zircon results. The unpolished AG10-02 included some anomalous ages resulting in a similar average age of 28.5 ± 0.3 Ma but with an MSWD of 11. Thus, at the level of ion microprobe U–Pb precision, no obviously xenocrystic component or discernable difference between the age of the last grown rim component relative to the core were identified.

^{40}Ar/^{39}Ar fusion and total-gas step-heating results for AG10-02 sanidine yield a weighted mean ^{40}Ar*/^{39}Ar ratio of 0.63189 ± 0.00019 (0.030%; 2σ), which is within uncertainty of the mean value of 0.63218 ± 0.00017 (0.027%; 2σ) determined from fusion analyses of co-irradiated Fish Canyon Tuff sanidine grains from the classic site (FC3). Step heating results for two multi-grain aliquots of AG10-02 sanidine from the distal quarry site are shown in Fig. 3 together with results for sample FC3 sanidine from the classic site from Phillips and Matchan (2013) for comparison. FC3 was a different sample to FCT-1, but from essentially the same locality. The two release spectra in Fig. 3 are indistinguishable and AG10-02 sanidine shows the same pattern of increasing age with progressive Ar release noted at the classic site by Phillips and Matchan (2013), which is revealed because of the very high precision of the analyses obtained with the ARGUS VI multi-collector mass spectrometer. Possible reasons for these rising spectra are discussed by Phillips and Matchan (2013), but the important conclusion here is that sanidines from the classic and distal sites, show essentially identical behaviour.

Zircon (U–Th)/He results for two of the four samples are shown in Table 4 and have weighted mean ages ranging from 26.9 ± 1.5 to 28.7 ± 0.4 Ma (1σ). The results were determined for between 3 and 30 single zircon grains per sample and include two each from the classic section and the distal sites. The mean ages are indistinguishable from each other and the reference age of 28.2 Ma, giving a weighted mean ZHe age for all four samples of 28.3 ± 0.4 Ma.

Apatite (U–Th–Sm)/He ages from the vertical section including the classic sampling site, yield an average weighted mean age from multiple analyses at the five sites that range from a low of 20.8 ± 0.4 Ma at the FCT-1 site to a high of 29.5 ± 1.2 Ma (1σ, Table 3). Taken by themselves, the four samples from the top ~100 m of the traverse cluster with an average age of 28.4 ± 0.2 Ma which is consistent with the reference age of 28.2 Ma and clearly distinct from the AHe age of FCT-1 some 280 m below at the classic site. This relationship is reasonable as the structurally highest samples are expected to be first to cool to closure following emplacement, but does clearly indicate that the classic site was within the He partial retention zone for apatite following emplacement.

In contrast, apatite fission track (AFT) ages from the same samples, range only from 28.8 ± 0.8 Ma (±1σ) at the classic site (2580 m) to an average of 27.4 ± 0.7 Ma for three of the higher samples (AG10-05 to -07) in the vertical section (2831–2856 m) (Table 5). These are indistinguishable and the weighted mean AFT age for all of these proximal samples is 28.1 ± 0.6 Ma. The highest sample in the vertical section (AG10-04 at 2913 m), however, has a significantly younger AFT age of 23.2 ± 1.7 Ma that is significantly different to the other samples in this section, and was excluded from the mean. This sample (AG10-04) shows clear evidence of some thermal disturbance with a significantly shortened mean track length of 13.96 ± 0.58 μm, compared to a weighted mean of 14.84 ± 0.04 μm for all other samples (Table 5, Fig. 4b). Only 19 confined track lengths were measured in AG10-04, but the distribution included two substantially shortened tracks of only 5 and 12 μm that are clear evidence that at least some of the grains have been disturbed.

The most likely explanation for the shortened track lengths and reduced AFT age for AG10-04 is that it has been superficially affected by a forest fire in the recent past. This sample was collected from a natural outcrop beside the road, unlike the other samples in this section that were from road cuts. The AHe age for this sample of 28.4 ± 0.3 Ma, shows no such reduction, however, despite the normally greater sensitivity of the AHe system. Two explanations are suggested for this inverted pattern, one being that the fire affected only a thin surface layer of the outcrop. The AHe age, being determined on only 4 hand-picked grains would be much less likely to sample apatites from this thin layer, compared to the AFT age, that was determined on 37 grains. The other is the apparent cross-over in the retentivity of the two systems noticed by Reiners et al. (2007) in apatites that had been partially reset on the short time scales of forest fire influence.

The retentivity of fission tracks in apatite is sensitive to compositional controls on annealing and track etchability (Cl and D_{par} content; Donelick et al., 2005). As Cl content in apatite can vary substantially in an evolving magmatic system (Fuge, 1977), variations in fission track retentivity between apatites are expected. Apatite D_{par} measurements and Cl content vary throughout the proximal and distal sample suite, but are highest (2.33 μm and 0.82 wt%, respectively) in apatites from FCT-1 at the classic site. The fission track retentivity of apatites from the classic site is therefore likely to be the highest of any of the samples studied. There is no correlation between the FT ages of individual apatite grains and either D_{par} or Cl content across all of the samples analysed but D_{par} and Cl content are highly correlated with each other (Fig. 4c), as expected for this compositional range.

The pattern of AFT ages argues strongly that, with the exception of AG10-04, none of the samples, in either the proximal section or the distal sites, show any disturbance after initial rapid cooling dating from the time of ignimbrite emplacement. This is confirmed by the radial plot (Fig. 4a) for all of the single grain AFT ages, which is consistent with a single age population, and the long, narrow track length distribution (Fig. 4b), which shows that all tracks were formed at low temperatures. The undisturbed nature of all the AFT ages (except AG10-04) is consistent with the likely maximum post-emplacement temperature near the bottom of the proximal cooling sheet of ~40–50 °C for a burial depth of ~1000 m and reasonable values for surface temperature and

Table 4
Fish Canyon Tuff – single grain zircon (U–Th)/He data.

Sample number	Lab. No.	He No.	^{4}He (ncc)	Mass (mg)	Mean F_T[a]	U (ppm)	Th (ppm)	Th/U	[eU] (ppm)[b]	Corrected age (Ma $\pm 1\sigma$)	Grain length (μm)	Grain radius (μm)
AG10-01	7014	20609	6.417	0.0086	0.77	100.7	165.8	1.65	139.6	44.0 ± 2.7[c]	311.2	45.3
AG10-01	7015	20611	5.578	0.0118	0.79	127.4	102.5	0.80	151.5	25.7 ± 1.6	386.9	48.3
AG10-01	7016	20613	13.306	0.0089	0.79	382.4	224.9	0.59	435.3	28.1 ± 1.7	289.5	46.7
AG10-01	7177	20721	3.894	0.0170	0.82	55.9	15.2	0.27	59.5	31.5 ± 2.0	395.7	51.2
AG10-01	7178	20726	24.566	0.0245	0.83	298.1	176.7	0.59	339.6	24.3 ± 1.5	479.2	57.9
									AG10-01 Weighted mean age	*26.9 ± 1.5*		
AG10-02	6832	20043	28.877	0.0068	0.77	816.2	948.4	1.16	1039.0	33.6 ± 2.1	248.8	39.2
AG10-02	6833	20045	17.620	0.0146	0.83	158.0	103.5	0.65	182.3	54.0 ± 3.3[c]	234.8	44.8
AG10-02	7017	20619	10.410	0.0098	0.76	276.8	200.8	0.73	324.0	26.9 ± 1.7	425.8	36.3
AG10-02	7018	20621	6.218	0.0085	0.77	199.5	138.2	0.69	232.0	26.0 ± 1.6	307.7	39.1
									AG10-02 Weighted mean age	*28.1 ± 2.2*		
AG10-04	6836	20056	13.179	0.0097	0.79	363.4	187.6	0.52	407.5	27.3 ± 1.7	367.3	47.0
AG10-04	6837	20058	17.854	0.0152	0.81	306.6	174.1	0.57	347.5	27.8 ± 1.7	309.9	43.5
AG10-04	6838	20060	21.849	0.0168	0.80	285.2	276.5	0.97	350.2	30.5 ± 1.9	455.9	43.8
									AG10-04 Weighted mean age	*28.4 ± 1.0*		
FCT-1	5336	15278	3.877	0.0053	0.74	198.3	134.9	0.68	230.0	26.0 ± 1.6	247.9	37.7
FCT-1	5337	15358	15.550	0.0127	0.83	315.0	175.8	0.56	356.4	28.1 ± 1.7	250.5	62.8
FCT-1	5800	16645	18.306	0.0121	0.81	328.7	225.8	0.69	381.8	32.6 ± 2.0	288.5	52.4
FCT-1	5801	16649	13.699	0.0122	0.82	281.5	156.6	0.56	318.3	28.9 ± 1.8	279.3	56.9
FCT-1	5933	19152	14.872	0.0119	0.82	322.3	171.4	0.53	362.6	28.2 ± 1.7	283.4	60.7
FCT-1	6628	19240	15.965	0.0094	0.80	403.7	219.9	0.54	455.4	30.7 ± 1.9	263.9	57.2
FCT-1	6863	20030	10.363	0.0073	0.79	363.0	178.3	0.49	404.9	28.9 ± 1.8	227.5	59.5
FCT-1	6864	20125	15.479	0.0080	0.80	460.5	242.9	0.53	517.5	30.6 ± 1.9	235.9	54.9
FCT-1	7012	20527	9.682	0.0131	0.82	200.4	125.6	0.63	229.9	26.3 ± 1.6	289.0	58.9
FCT-1	7013	20534	10.542	0.0085	0.77	325.1	179.5	0.55	367.3	27.8 ± 1.7	311.9	39.3
FCT-1	7176a	20708	13.096	0.0084	0.79	359.0	281.6	0.78	425.2	30.2 ± 1.9	245.5	48.7
FCT-1	7864	23554	14.304	0.0074	0.79	521.7	269.7	0.52	585.1	27.0 ± 1.7	234.6	49.6
FCT-1	8139	24034	18.606	0.0149	0.81	284.3	139.6	0.49	317.1	32.4 ± 2.0	315.6	59.0
FCT-1	8393	25197	11.315	0.0120	0.82	247.8	134.7	0.54	279.5	27.6 ± 1.7	273.5	58.6
FCT-1	8394	25753	13.112	0.0092	0.80	351.4	178.4	0.51	393.3	29.7 ± 1.8	253.7	52.9
FCT-1	8620	25857	9.170	0.0070	0.78	364.3	253.0	0.69	423.7	25.3 ± 1.6	238.3	47.1
FCT-1	8667	26012	16.677	0.0127	0.81	294.5	183.0	0.62	337.5	31.8 ± 2.0	326.5	52.2
FCT-1	8689	26107	17.479	0.0143	0.82	266.5	169.9	0.64	306.4	32.6 ± 2.0	341.6	54.2
FCT-1	8902	26792	6.113	0.0051	0.76	401.2	195.7	0.49	447.2	28.5 ± 1.8	207.9	43.8
FCT-1	8966	26994	5.369	0.0097	0.78	197.0	120.9	0.61	225.4	25.8 ± 1.6	345.1	43.0
FCT-1	8966A	27035	8.109	0.0084	0.79	305.5	179.5	0.59	347.7	28.5 ± 1.8	253.2	50.2
FCT-1	9149	27494	13.782	0.0079	0.79	424.3	223.9	0.53	476.9	30.0 ± 1.9	250.2	48.7
FCT-1	9214	27668	14.360	0.0102	0.80	359.2	182.2	0.51	402.0	28.8 ± 1.8	279.6	51.7
FCT-1	9225	27727	10.276	0.0145	0.83	184.9	106.5	0.58	210.0	27.6 ± 1.7	316.6	58.6
FCT-1	9232	27737	11.247	0.0061	0.78	441.6	220.3	0.50	493.4	30.8 ± 1.9	253.6	45.8
FCT-1	9233	27764	20.044	0.0134	0.82	348.4	184.7	0.53	391.8	31.4 ± 1.9	312.7	58.0
FCT-1	9254	27932	19.434	0.0097	0.82	519.1	304.5	0.59	590.7	27.8 ± 1.7	298.2	55.9
FCT-1	9424	28409	14.069	0.0093	0.79	299.4	177.0	0.59	341.0	36.5 ± 2.3[c]	289.7	47.6
FCT-1	9515	28695	10.880	0.0059	0.77	522.0	229.9	0.44	576.1	26.4 ± 1.6	231.3	43.4
FCT-1	9609	28910	6.585	0.0041	0.73	376.7	242.6	0.64	433.7	30.5 ± 1.9	214.5	37.0
									FCT-1 Weighted mean age	*28.7 ± 0.4*		

[a] F_T is the a-ejection correction after Farley et al. (1996).
[b] Effective uranium content [U ppm + 0.235 * Th ppm].
[c] Analysis not included in weighted average age calculation.

thermal gradient. The lack of observable post emplacement fission track annealing at the classic site is enhanced by the high Cl content for apatites at this locality, justifying its use as an AFT standard (Naeser et al., 1981; Hurford and Green, 1982).

In contrast, the AHe ages for FCT-1 apatites at the classic site provide clear evidence for significant post-eruptive, probably Early Miocene, cooling near the base of the ignimbrite sheet through the temperature range ~70–40 °C. We attribute this protracted duration of cooling in this area to km-scale erosion, possibly triggered by structural changes related to formation of the nearby Rio Grande Rift.

At the three distal localities, some 35–45 km to the east of the classic site, where the FCT is only about 40–100 m thick, the average weighted mean AHe ages range from 27.7 ± 1.4 Ma to 28.6 ± 0.6 Ma ($\pm 1\sigma$), with a weighted mean age of 28.5 ± 0.2 Ma. These ages are within uncertainties of the AFT ages for these three localities (28.3 ± 1.6 Ma to 30.1 ± 3.3 Ma, weighted mean 28.5 ± 0.3 Ma) as well as the broadly known age of FCT eruption (~28 Ma; Steven et al., 1967; Bachmann et al., 2007). Thus the three distal sites show no evidence of later cooling or other thermal disturbance after the time of initial emplacement. The weighted mean of all of the AHe ages (except FCT-1) and all the AFT ages (except AG10-04) at both proximal and distal sites is 28.4 ± 0.1 Ma.

Amongst the distal samples, the lithic-poor sample AG10-02 yielded more precise AHe and AFT ages and was excavated from a fresh quarry making this a promising candidate for use as a standard that will satisfy the requirements of both the AHe and AFT thermochronometry systems. This new quarry site has essentially identical behaviour in the high-temperature systems and the AFT system to the classic site, but is notably superior for the low-temperature AHe system.

Table 5
Fish Canyon Tuff – (U–Th–Sm)/He apatite data.

Sample No.	Lab ID No.	He No.	^{4}He (ncc)	No. of grains	Crystal form[a]	Mass (mg)	F_T[b]	U (ppm)	Th (ppm)	Sm (ppm)	Th/U ratio	[eU] (ppm)[c]	Corrected age (Ma $\pm 1\sigma$)	Crystal length (μm)	Crystal radius (μm)
AG10-01	6261	18295	0.130	1	1T	0.0049	0.74	3.6	27.3	296.8	7.51	10.0	28.1 ± 1.7	213.0	58.2
AG10-01	6262	18298	0.124	1	1T	0.0042	0.73	5.1	27.3	280.5	5.32	11.5	28.2 ± 1.8	209.6	53.8
AG10-01	6748	19718	0.395	1	0T	0.0078	0.76	10.4	42.6	127.3	4.09	20.4	26.7 ± 1.7	261.4	54.4
AG10-01	6749	19720	0.299	1	0T	0.0055	0.73	9.4	44.6	167.7	4.75	19.9	30.7 ± 1.9	238.7	47.8
													AG10-01 Weighted mean age	*28.3 ± 0.8*	
AG10-02	5952	17354	1.465	1	1T	0.0214	0.84	12.1	50.3	161.9	4.15	23.9	27.6 ± 1.7	337.7	97.0
AG10-02	5953	17359	1.447	1	1T	0.0179	0.84	13.8	56.6	196.1	4.11	27.1	29.0 ± 1.8	304.4	94.3
AG10-02	5954	17362	1.510	1	0T	0.0224	0.83	12.0	49.1	155.9	4.09	23.5	27.9 ± 1.7	320.0	83.5
AG10-02	5955	17365	1.742	1	0T	0.0230	0.83	9.6	41.2	128.7	4.28	19.3	38.2 ± 2.4[d]	321.0	84.5
AG10-02	6017	17559	2.488	1	0T	0.0306	0.84	14.0	53.6	186.0	3.82	26.6	29.4 ± 1.8	413.8	85.8
AG10-02	6322	18469	1.283	1	0T	0.0113	0.82	21.3	84.3	307.0	3.97	41.1	27.5 ± 1.7	233.7	88.3
AG10-02	6324	18563	1.282	1	0T	0.0169	0.84	13.3	53.7	172.0	4.03	25.9	28.4 ± 1.8	308.8	90.5
AG10-02	6323	18566	1.265	1	0T	0.0125	0.82	17.8	75.1	263.6	4.22	35.4	28.4 ± 1.8	275.1	82.5
AG10-02	6663	19452	0.634	1	1T	0.0092	0.78	12.3	48.1	182.2	3.90	23.6	30.6 ± 1.9	324.8	62.4
AG10-02	6750	19722	1.159	1	1T	0.0139	0.82	14.6	57.9	234.4	3.97	28.2	29.4 ± 1.8	311.2	80.5
AG10-02	6751	19701	1.004	1	2T	0.0157	0.80	12.0	46.7	164.0	3.88	23.0	28.4 ± 1.8	361.7	72.3
													AG10-02 Weighted mean age	*28.6 ± 0.3*	
AG10-03	6265	18312	0.066	1	0T	0.0024	0.67	5.5	31.5	351.5	5.76	12.9	25.4 ± 1.6	116.4	45.3
AG10-03	6266	18315	0.078	1	0T	0.0028	0.68	4.5	30.2	438.2	6.73	11.6	27.7 ± 1.7	124.7	47.5
AG10-03	6267	18318	0.190	1	1T	0.0030	0.68	11.1	72.1	679.9	6.48	28.0	26.8 ± 1.7	227.8	42.4
AG10-03	6268	18321	0.067	1	2T	0.0023	0.62	4.7	28.3	314.2	6.09	11.4	32.5 ± 2.0	184.3	39.1
													AG10-03 Weighted mean age	*27.7 ± 1.4*	
AG10-04	6269	18324	0.463	1	1T	0.0054	0.76	15.1	63.0	241.2	4.17	29.9	30.8 ± 1.9	214.7	61.1
AG10-04	6270	18327	0.308	1	1T	0.0057	0.77	11.1	48.6	162.9	4.38	22.5	25.6 ± 1.6	214.6	62.9
AG10-04	6271	18330	0.305	1	1T	0.0052	0.76	11.5	49.4	161.7	4.28	23.1	27.4 ± 1.7	195.2	63.8
AG10-04	6272	18333	1.038	1	0T	0.0245	0.84	7.9	29.9	98.3	3.80	14.9	27.4 ± 1.7	195.9	111.6
													AG10-04 Weighted mean age	*27.6 ± 1.0*	
AG10-05	6273	18336	0.250	1	1T	0.0040	0.75	11.4	53.0	164.5	4.67	23.9	28.7 ± 1.8	153.3	66.2
AG10-05	6274	18339	0.596	1	0T	0.0128	0.81	8.3	33.5	133.9	4.04	16.2	29.0 ± 1.8	151.8	91.5
AG10-05	6275	18342	0.567	1	1T	0.0073	0.79	15.0	59.3	186.6	3.96	28.9	27.9 ± 1.7	207.4	74.5
AG10-05	6276	18345	0.287	1	1T	0.0041	0.75	13.8	57.7	179.6	4.19	27.4	28.1 ± 1.7	175.3	60.3
													AG10-05 Weighted mean age	*28.4 ± 0.3*	
AG10-06	6277	18348	0.800	1	1T	0.0077	0.79	18.6	77.2	255.2	4.14	36.7	29.2 ± 1.8	233.8	70.5
AG10-06	6278	18351	0.387	1	0T	0.0078	0.78	10.2	37.7	135.9	3.69	19.1	27.1 ± 1.7	175.7	66.6
AG10-06	6279	18354	0.593	1	1T	0.0077	0.80	12.8	49.9	171.4	3.89	24.5	31.9 ± 2.0	195.3	81.2
AG10-06	6280	18357	0.310	1	0T	0.0082	0.78	7.7	28.2	107.4	3.66	14.3	27.6 ± 1.7	202.4	63.6
													AG10-06 Weighted mean age	*28.7 ± 1.0*	
AG10-07	6282	18363	0.278	1	1T	0.0052	0.76	9.5	44.5	146.9	4.67	20.0	29.0 ± 1.8	210.9	60.3
AG10-07	6283	18366	0.402	1	0T	0.0075	0.77	9.0	36.2	141.1	4.02	17.5	32.3 ± 2.0	150.6	70.2
AG10-07	6746	19706	2.824	1	1T	0.0190	0.83	26.4	37.9	136.4	1.44	35.3	41.5 ± 2.1[d]	328.1	76.0
AG10-07	6747	19708	0.884	1	0T	0.0188	0.83	8.7	31.9	130.6	3.65	16.2	28.2 ± 1.5	232.0	89.7
													AG10-07 Weighted mean age	*29.5 ± 1.2*	
FCT-1	2277	5892	0.261	3	0T, 0T, 1T	0.0105	0.72	5.9	27.4	84.2	4.67	12.3	23.0 ± 1.4	116.5	60.2[e]
FCT-1	2278	5874	0.221	3	1T, 0T, !T	0.0067	0.68	10.4	36.2	124.5	3.47	18.9	20.9 ± 1.3	116.5	51.5[e]
FCT-1	2279	5895	0.362	3	0T, 0T, 1T	0.0076	0.68	8.5	32.6	113.5	3.85	16.2	35.5 ± 2.2[d]	127.9	48.2[e]
FCT-1	6114	17824	0.771	1	0T	0.0160	0.81	15.6	36.4	118.4	2.33	24.2	20.2 ± 1.3	387.9	64.1
FCT-1	6115	17842	0.947	1	1T	0.0193	0.81	15.9	42.6	129.8	2.68	25.9	19.2 ± 1.2	566.2	66.7
FCT-1	6116	17839	1.813	1	1T	0.0340	0.84	17.6	42.9	138.8	2.44	27.7	18.8 ± 1.2	697.9	79.7
FCT-1	6117	17836	0.946	1	2T	0.0148	0.80	20.5	51.1	151.4	2.50	32.5	20.1 ± 1.3	307.6	76.2
FCT-1	6118	17833	0.976	1	1T	0.0159	0.83	15.7	45.1	142.7	2.88	26.3	23.1 ± 1.4	336.5	82.3
FCT-1	6661	19457	1.083	1	0T	0.0221	0.84	14.5	35.1	113.4	2.41	22.7	21.0 ± 1.3	331.0	81.5
FCT-1	6195	18089	0.977	1	1T	0.0122	0.81	22.5	65.8	200.7	2.92	38.0	21.3 ± 1.3	339.1	71.0
FCT-1	6196	18092	2.322	1	2T	0.2690	0.84	2.3	6.7	20.7	2.96	3.9	21.9 ± 1.4	382.0	92.1
FCT-1	6197	18095	0.868	1	2T	0.0172	0.81	15.2	40.8	119.1	2.68	24.8	20.6 ± 1.3	342.1	77.7
													FCT-1 Weighted mean age	*20.8 ± 0.4*	

[a] Crystal form – 0T = no crystal terminations, 1T = one crystal termination and 2T = 2 crystal terminations.
[b] F_T is the α-ejection correction after Farley et al. (1996).
[c] Effective uranium content [U ppm + 0.235 * Th ppm].
[d] Analysis not included in determination of weighted mean age.
[e] Mass weighted average radius of apatite crystals (where more than one was analysed) measured in the aliquot analysed.

Table 6
Fish Canyon Tuff – apatite fission track results.

Sample No.	Elevation (m)	No. of grains	N_s	ρ_s ($\times 10^5$ cm^{-2})	^{238}U (ppm)	D_{par} (μm)	Cl (wt%)	$P(\chi^2)$ (%)	Pooled age (Ma ± 1σ)	Central age (Ma ± 1σ)	N_{length}	Mean track length (μm ± 1σ)	St. dev. (μm)
Distal sites:													
AG10-01	2418	38	373	1.819	12.98	2.10	0.63	26.6	28.4 ± 1.6	28.3 ± 1.6	97	14.64 ± 0.10	0.96
AG10-02A	2467	36	548	1.817	13.65	2.10	0.70	49.7	26.8 ± 1.3	26.7 ± 1.2	–	–	–
AG10-02B	2467	36	656	2.081	13.94	1.98		22.6	30.0 ± 1.1	29.9 ± 1.3	–	–	–
AG10-02 Comb.	2467	72	1204	1.952	13.80	2.04	0.70	34.3	28.4 ± 0.9	28.4 ± 0.9	117	15.00 ± 0.09	0.92
AG10-03	2543	21	98	0.993	6.61	2.01	0.66	43.7	30.0 ± 3.0	30.1 ± 3.3	–	–	–
Proximal section:													
AG10-04	2913	37	209	1.473	12.76	2.07	0.65	57.7	23.2 ± 1.9	23.2 ± 1.7	19	13.96 ± 0.58	2.47
AG10-05	2856	42	771	2.097	14.93	2.16	0.70	31.4	28.2 ± 1.1	28.2 ± 1.1	108	14.82 ± 0.10	0.95
AG10-06	2847	42	358	1.883	13.65	2.29	0.73	44.5	27.7 ± 1.6	27.6 ± 1.6	107	14.68 ± 0.10	0.96
AG10-07	2831	40	445	1.778	13.79	2.06	0.67	53.7	25.9 ± 1.6	25.9 ± 1.5	128	14.96 ± 0.09	0.92
Classic site:													
FCT-1A	2580	42	715	1.875	13.49	2.33	0.82	31.1	28.0 ± 1.3	27.9 ± 1.2	–	–	–
FCT-1B	2580	37	833	2.276	15.43	2.33	0.81	35.2	29.7 ± 1.3	29.6 ± 1.1	–	–	–
FCT-1 Comb.	2580	79	1548	2.071	14.44	2.33	8.82	28.9	28.8 ± 0.9	28.8 ± 0.8	112	14.86 ± 0.09	0.87
All results combined:													
All samples[a]		334	4797	1.935	13.78	2.16	0.72	64.0	28.2 ± 0.5	28.2 ± 0.4	585	14.84 ± 0.04	0.86

N_s = number of spontaneous tracks counted; ρ_s = spontaneous track density; D_{par} = long axis of track etch pit; N_{length} = number of lengths measured; se = standard error.
[a] Except AG10-04.

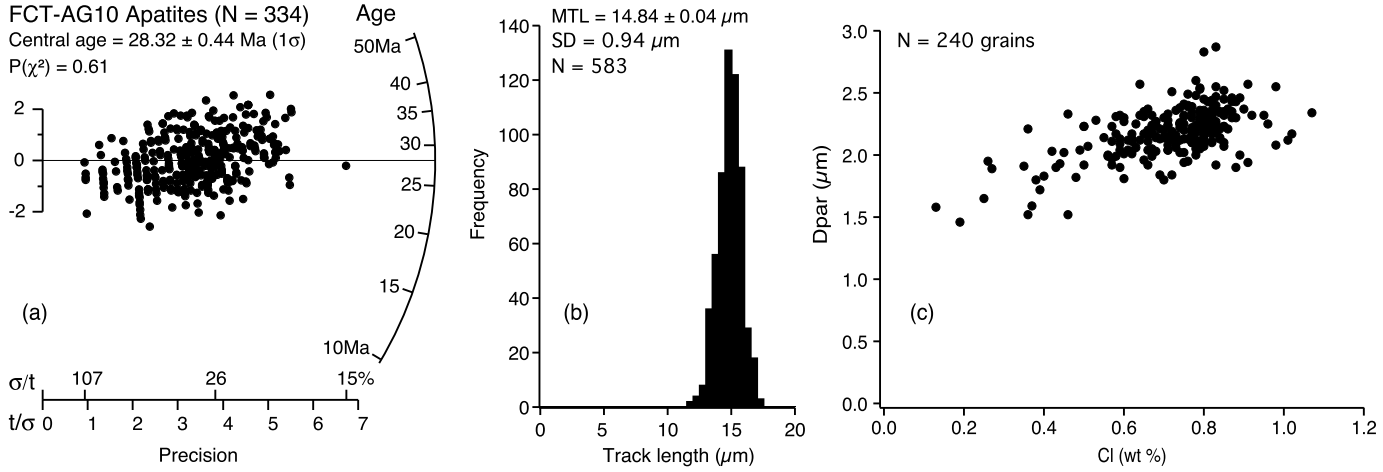

Fig. 4. Apatite fission track data for all the Fish Canyon Tuff apatite samples analysed in this study, except AG10-04. **(a)** Radial Plot showing the variation of single grain fission track ages for 334 apatite grains. The vertical axis shows the uncertainties of ±2σ against relative precision for each grain on the horizontal axis. The age is given by a line drawn from the origin to the radial scale on the right for each grain, the horizontal line representing a reference age of 28 Ma. On this plot error bars are the same height for all the grains and it can be seen that the distribution of single grain results is consistent with a single age population at 95% confidence limits. The quantized nature of the points, especially visible on the left side of the diagram, is a consequence of the discrete counts of fission tracks in individual grains at low track numbers. **(b)** The length distribution for 583 confined fission tracks measured as the true 3D length of confined tracks dipping at up to 20° to the surface. For such relatively low dips, these depth-corrected length measurements are regarded as comparable to uncorrected 'horizontal' confined track lengths. **(c)** Variation of the track etch-rate parameter D_{par} with apatite Cl concentration for 240 apatite grains analysed in this study. These two parameters are highly correlated for this sample set, although single grain ages showed no variation with either of these parameters, which is consistent with the inferred thermal history of residence at low, near surface, temperatures since initial rapid cooling following ignimbrite emplacement.

4. Conclusions

Fission track and (U–Th–Sm)/He apatite dating of a suite of samples from the 28 Ma Fish Canyon Tuff (FCT) ignimbrite sheet, southwestern Colorado, show generally concordant ages at a weighted mean 28.4 ± 0.1 Ma (all 1σ se), with the exception of the classic sampling locality on Colorado Highway 160. At the classic site, the (U–Th–Sm)/He apatite age is 20.8 ± 0.4 Ma which is ~7 Ma younger than the apatite fission track age of 28.8 ± 0.8 Ma and indicative of protracted post-eruption cooling in the temperature range of ~40–60 °C until at least early Miocene time at this locality.

AHe and AFT apatite ages from a ~330 m vertical section through the FCT immediately above the classic sampling location are all consistent with the time of ignimbrite emplacement, except for the uppermost sample, AG10-04, where the AFT age is reduced to 23.2 ± 1.7 Ma, but not the AHe age (28.4 ± 1.7 Ma). It is suggested that this sample, from a natural outcrop, appears to have been partially influenced by a local thermal disturbance, most probably a forest fire. The apatites from the classic locality exhibit the highest average Cl concentrations of any of the apatites sampled, leading to enhanced retentivity of fission tracks in this sample and helping to explain the concordance of the AFT age at this site, despite the substantially reduced AHe age. Fish Canyon Tuff from the classic site is therefore only partially suitable as an age standard for low-temperature thermochronometers, as might be expected from its position near the bottom of a ~1000 m volcanic pile.

At three distal locations about 35–45 km NE to SE of the classic site, where the total FCT thickness was less than ~100 m, AHe and AFT ages average 28.5 ± 0.1 Ma, indistinguishable from each

other and the time of eruption. Zircon (U–Th)/He ages from four samples, two distal and two proximal, are all concordant with a weighted mean of 28.5 ± 0.2 Ma.

One of these distal sites (sample AG10-02) is a quarry near the top of the Fish Canyon Tuff ignimbrite sheet where an abundance of fresh material is available with identical mineralogy and texture to the classic locality, but with many fewer lithic clasts. The total thickness of the FCT itself at this locality is only ~40 m, most of it below the quarry, and the estimated thickness of all overlying units is <150 m, so that it satisfies the geological requirements for an age standard to a much greater degree than the classic proximal site. U–Pb zircon ages and $^{40}Ar/^{39}Ar$ sanidine ages from this distal site show identical behaviour to material from the classic locality, despite contrasting amounts of lithic inclusions between the two sites. On this basis we suggest that the new distal quarry site provides a source of age standard material that is superior to the classic site in that it is suitable for both high-temperature systems and all of the low-temperature thermochronometers in the fission track and (U–Th–Sm)/He systems.

Acknowledgements

The ion microprobe facility at the University of California, Los Angeles, is partly supported by a grant from the Instrumentation and Facilities Program, Division of Earth Sciences, National Science Foundation. N9547N provided outstanding logistic support during fieldwork. Abaz Alimanovic is thanked for technical support for mineral separations, helium analyses, and solution ICP-MS analyses. Christian Seiler and Ling Chung provided valuable assistance with various aspects of the fission track analyses and LA-ICP-MS analyses. We also thank two anonymous reviewers for their constructive comments. The Automated Fission Track Analysis Facility at the University of Melbourne was developed with support from Australian Research Council Grants LP0348767 and LE0882818 and additional operational and equipment funding from the National Collaborative Research Infrastructure Strategy AuScope program and the Education Investment Fund AGOS program.

Appendix A. Detailed fission track analytical methods

All microscopy for fission track analysis was carried out using motorised *Zeiss* M1m microscopes fitted with *Autoscan* ES16 scanning stages and AVT Oscar 3.3 MP CCD digital cameras, interfaced to a control PC operating the in-house developed *TrackWorks* microscope control software system. The focus control on the Z1m is extremely precise and allows vertical movements in increments of 25 nm. All measurements were made on digital image sets captured by the system using a 100× dry objective and archived to disk for later retrieval and processing using *FastTracks* image analysis and measurement software at an effective magnification of the digital images on-screen of ~2000× for track count mode and ~8000× for length measurement mode.

Two polished mounts were prepared for each sample. The first was used for the determination of the fission track age and the second for track length measurement. Three electron microscope Cu grids cemented to each slide were used to establish an internal coordinate system, these markers being automatically located and recorded by *TrackWorks*. The polished and etched mounts were also coated with a thin Au film (~10 nm) using a sputter coating unit to enhance the surface reflectivity as described by Gleadow et al. (2009). About 40 grains with c-axes lying horizontally in the plane of the polished surface were selected for counting using circular polarised light and an automated grain detection option in *TrackWorks*. Reflected and transmitted light digital image sets were then captured autonomously and analysed offline using *FastTracks* image processing software. Spontaneous fission tracks were counted automatically using the coincidence mapping procedure described by Gleadow et al. (2009) and then manually corrected as necessary. The c-axis direction was determined automatically and corrected manually as necessary. Average D_{par} values (Donelick et al., 2005) for all single-track etch pits were also determined automatically, taking about 10 s for the analysis over all measured grains in each mount. Cl concentrations were determined by electron microprobe.

The second apatite mount was exposed to a ^{252}Cf fission source in a vacuum chamber to enhance the number of confined track intersections below the surface (Donelick and Miller, 1991). These irradiations gave an implanted track density of $\sim 8 \times 10^6$ cm^{-2} at a distance of 1 cm from the source providing collimated Cf tracks incident approximately normal to the surface. Digital image z-stacks, with 0.3–0.5 μm spacing, were captured autonomously in both transmitted and reflected light at locations of confined tracks previously identified by the operator using *TrackWorks*. The true lengths of ~100 confined tracks were then measured in 3D on the retrieved image sets for shallow dipping tracks up to 20° using *FastTracks*, correcting the vertical component for a refractive index of 1.634 for apatite (Laslett et al., 1982). The resulting length data are more precise but comparable to traditional 'horizontal' confined track lengths where only the horizontal length component is measured for shallow dipping tracks up to 10–15° (Ketcham et al., 2009; Laslett et al., 1982).

Uranium concentrations were measured by LA-ICP-MS using a New Wave UP-213 Quintupled Nd:YAG Laser Microprobe and an Agilent 7700X ICP-MS. For each apatite grain 3–4 laser spots of 30 μm diameter were ablated to a depth of ~8 μm in a 'Supercell' under He, with Ar as the carrier gas. The 213 nm laser was used with a pulse rate of 5 Hz and 45% power giving an energy density of 2.3 J/cm^2 at the target. Measurements were made on the $^{238}U/^{43}Ca$ ratio against glass (NIST612) and a homogenised and recrystallised Mud Tank Carbonatite apatite standard. Repeat analyses of a Durango apatite reference crystal were also included with the FCT runs as an additional internal standard. Internal consistency in the ^{238}U measurements between the multiple spots was generally excellent, but a few grains were rejected where the repeat analyses exceeded experimental error.

Fission track ages were calculated as described by Hasebe et al. (2004) using an absolute calibration based on primary constants rather than an empirical calibration, although the results presented here show that the two approaches are essentially equivalent. Pooled ages were calculated for each sample from the spontaneous track density over all grains (total tracks over total area counted), and the average ^{238}U concentration weighted according to the area counted over each grain. Central ages were also calculated using the *RadialPlotter* package (Vermeesch, 2009). Ages were determined from the following equation, after Hasebe et al. (2004):

$$t = \frac{1}{\lambda_D}\left(1 + \ln \lambda_D \xi \frac{\rho_s}{C_U}\right) \quad (1)$$

where t is the fission track age, ρ_s = spontaneous track density (cm^{-2}), C_U = concentration of ^{238}U, and λ_D = total (alpha) decay constant for ^{238}U (1.55125×10^{-10} yr^{-1}, Jaffey et al., 1971). The value of ξ used in this study is 2.010×10^{-3} determined by calibration against age standards, equivalent to the conventional zeta-calibration approach.

The constants making up this aggregate ξ factor, however, are given by:

$$\xi = \frac{A}{\lambda_f N_0 D R \alpha} \quad (2)$$

where A = atomic weight of ^{238}U, λ_f = spontaneous fission decay constant for ^{238}U, N_0 = Avogadro's number, D = density of

apatite, R = etchable range of one fission fragment, and α = the detection efficiency of the etched internal apatite surface.

All of these constants in Eq. (2) can be individually evaluated, with A and N_0 being known very precisely. For D, we use a value of 3.21 derived from a calculated relationship between density and apatite Cl content based on the analyses and unit cell dimensions of Carlson et al. (1999). R may be taken as 7.5 μm based on half the confined track length for spontaneous fission tracks in volcanic apatites (Gleadow et al., 1986). Despite much controversy in past decades about the spontaneous fission decay constant, λ_f, a consensus has emerged around the IUPAC recommended value of 8.5×10^{-17} yr^{-1} based on a weighted mean of the most precise and more recent values (Holdren and Hoffman, 2000). We have adjusted this value slightly to 8.52×10^{-17} yr^{-1} by including several more recent measurements cited by Yoshioka et al. (2005). The remaining factor α, the detection efficiency, defined as the fraction of fission tracks crossing a surface that are revealed by etching and counted by the observation system, is the most poorly known. This factor is likely to show differences between various laboratories and observers, although we find that using our automated counting system such differences are minimal. The relatively few direct measurements of this efficiency factor range from 0.90–0.99 (e.g. Iwano et al., 1993; Jonckheere and Van den haute, 2002). Hasebe et al. (2004) used a value of 1.0. Clearly more experimental work is needed to define this parameter with the counting setup used, but for this discussion a value of 0.96 is used. Combining these values gives $\xi = 2.07 \pm 0.07 \times 10^{-3}$, which is indistinguishable from the empirical value, and also within error of the value used by Hasebe et al. (2004). This discussion suggests that an absolute rather than a purely empirical calibration for fission track analysis is now possible.

References

Bachmann, O., Bergantz, G.W., 2003. Rejuvenation of the Fish Canyon magma body: a window into the evolution of large-volume silicic magma systems. Geology 31, 789–792.

Bachmann, O., Dungan, M.A., Lipman, P.W., 2000. Voluminous lava-like precursor to a major ash-flow tuff: low-column pyroclastic eruption of the Pagosa Peak Dacite, San Juan volcanic field, Colorado. J. Volcanol. Geotherm. Res. 98, 153–171.

Bachmann, O., Dungan, M.A., Lipman, P.W., 2002. The Fish Canyon magma body, San Juan Volcanic Field, Colorado: rejuvenation and eruption of an upper-crustal batholith. J. Petrol. 43, 1469–1503.

Bachmann, O., Oberli, F., Dungan, M.A., Meier, M., Mundil, R., Fischer, H., 2007. ^{40}Ar/^{39}Ar and U–Pb dating of the Fish Canyon magmatic system, San Juan Volcanic field, Colorado: evidence for an extended crystallization history. Chem. Geol. 236, 134–166.

Baksi, A.K., Archibald, D.A., Farrar, E., 1996. Intercalibration of ^{40}Ar/^{39}Ar dating standards. Chem. Geol. 129, 307–324.

Boehnke, P., Harrison, T.M., 2014. A meta-analysis of geochronologically relevant half-lives: what's the best decay constant? Int. Geol. Rev. http://dx.doi.org/10.1080/00206814.2014.908420.

Carlson, W.D., Donelick, R.A., Ketcham, R.A., 1999. Variability of apatite fission-track annealing kinetics: I. Experimental results. Am. Mineral. 84, 1213–1223.

Carpena, J., Mailhé, D., 1987. Fission track dating calibration of the Fish Canyon standard in French reactors. Chem. Geol. (Isotope Geosci.) 66, 53–59.

Cebula, G.T., Kunk, M.J., Mehnert, H.H., Naeser, C.W., Obradovich, J.D., Sutter, J.F., 1986. The Fish Canyon Tuff, a potential standard for the ^{40}Ar/^{39}Ar and fission-track dating methods. Terra Cognita 6, 139–140.

Daze, A., Lee, J.K.W., Villeneuve, M., 2003. An intercalibration study of the Fish Canyon sanidine and biotite ^{40}Ar/^{39}Ar standards and some comments on the age of the Fish Canyon Tuff. Chem. Geol. 199, 111–127.

Dobson, K.J., Stuart, F.M., Dempster, T.J., EIMF, 2008. U and Th zonation in Fish Canyon Tuff zircons: implications for a zircon (U–Th)/He standard. Geochim. Cosmochim. Acta 72, 4745–4755.

Donelick, R.A., Miller, D.S., 1991. Enhanced TINT fission track densities in low spontaneous track density apatites using ^{252}Cf-derived fission fragment tracks: a model and experimental observations. Nucl. Tracks Radiat. Meas. 18, 301–307.

Donelick, R.A., O'Sullivan, P.B., Ketcham, R.A., 2005. Apatite fission-track analysis. Rev. Mineral. Geochem. 58, 49–94.

Farley, K.A., Wolf, R.A., Silver, L.T., 1996. The effects of long alpha-stopping distances on (U–Th)/He ages. Geochim. Cosmochim. Acta 60, 4223–4229.

Fuge, R., 1977. On the behaviour of fluorine and chlorine during magmatic differentiation. Contrib. Mineral. Petrol. 61, 245–249.

Gleadow, A.J.W., Duddy, I.R., Green, P.F., Lovering, J.F., 1986. Confined fission track lengths in apatite – a diagnostic tool for thermal history analysis. Contrib. Mineral. Petrol. 94, 405–415.

Gleadow, A.J.W., Gleadow, S.J., Belton, D.X., Kohn, B.P., Krochmal, M.S., 2009. Coincidence mapping a key strategy for automated counting in fission track dating. In: Ventura, B., Lisker, F., Glasmacher, U.A. (Eds.), Thermochronological Methods: from Palaeotemperature Constraints to Landscape Evolution Models. Geol. Soc. (Lond.) Spec. Publ., vol. 324, pp. 25–36.

Hasebe, N., Barberand, J., Jarvis, K., Carter, A., Hurford, A.J., 2004. Apatite fission-track chronometry using laser ablation ICP-MS. Chem. Geol. 207, 135–145.

Holdren, N.E., Hoffman, D.C., 2000. Spontaneous fission half-lives for ground-state nuclides. Pure Appl. Chem. 72, 1525–1562.

Hourigan, J.K., Reiners, P.W., Brandon, M.T., 2005. U–Th zonation-dependent alpha-ejection in (U–Th)/He chronometry. Geochim. Cosmochim. Acta 69, 3349–3365.

House, M.A., Farley, K.A., Stockli, D., 2000. Helium chronometry of apatite and titanite using Nd–Yag laser heating. Earth Planet. Sci. Lett. 183, 365–368.

Hurford, A.J., Green, P.F., 1982. A users' guide to fission track dating calibration. Earth Planet. Sci. Lett. 59, 343–354.

Hurford, A.J., Hammerschmidt, K., 1985. ^{40}Ar/^{39}Ar and K/Ar Dating of the Bishop and Fish Canyon Tuffs: calibration of ages for fission-track dating standards. Chem. Geol. 58, 23–32.

Iwano, H., Kasuya, M., Danhara, T., Yamashita, T., Tagami, T., 1993. Track counting efficiency and unetchable track range in apatite. Nucl. Tracks Radiat. Meas. 21, 513–517.

Jaffey, A.H., Flynn, K.F., Glendenin, L.E., Bentley, W.C., Essling, A.M., 1971. Precision measurement of the half-lives and specific activities of ^{235}U and ^{238}U. Phys. Rev. 4, 1889–1906.

Jonckheere, R., Van den haute, P., 2002. On the efficiency of fission-track counts in an internal and external apatite surface and in a muscovite external detector. Radiat. Meas. 35, 29–40.

Jourdan, F., Renne, P.R., 2007. Age calibration of the Fish Canyon sanidine ^{40}Ar/^{39}Ar dating standard using primary K–Ar standards. Geochim. Cosmochim. Acta 71, 387–402.

Ketcham, R.A., Donelick, R.A., Balestrieri, M.L., Zattin, M., 2009. Reproducibility of apatite fission track length data and thermal history reconstruction. Earth Planet. Sci. Lett. 284, 504–515.

Kuiper, K.F., Deino, A., Hilgen, F.J., Krijgsman, W., Renne, P.R., Wijbrans, J.R., 2008. Synchronizing rock clocks of Earth history. Science 320, 500–504.

Lanphere, M., 2004. Reply to comment on "Precise K–Ar, ^{40}Ar/^{39}Ar, Rb–Sr and U–Pb mineral ages from the 27.5 Ma Fish Canyon Tuff reference standard" by M.A. Lanphere and H. Baadsgaard. Chem. Geol. 211, 389–390.

Lanphere, M.A., Baadsgaard, H., 1997. The Fish Canyon Tuff – a standard for geochronology. Eos 78, S326.

Lanphere, M.A., Baadsgaard, H., 2001. Precise K–Ar, ^{40}Ar/^{39}Ar, Rb–Sr and U/Pb mineral ages from the 27.5 Ma Fish Canyon Tuff reference standard. Chem. Geol. 175, 653–671.

Lanphere, M.A., Dalrymple, G.B., 2000. First-principles calibration of ^{38}Ar tracers: implications for the ages of ^{40}Ar/^{39}Ar fluence monitors. U.S. Geol. Surv. Prof. Pap. 1621, 1–10.

Laslett, G.M., Kendall, W.S., Gleadow, A.J.W., Duddy, I.R., 1982. Bias in measurement of fission track length distributions. Nucl. Tracks 6, 79–85.

Lee, J.-Y., Marti, K., Severinghaus, J.P., Kawamura, K., Yoo, H.-S., Lee, J.B., Kim, J.S., 2006. A redetermination of the isotopic abundances of atmospheric Ar. Geochim. Cosmochim. Acta 70, 4507–4512.

Lipman, P., Steven, T.A., Meinert, H.H., 1970. Volcanic history of the San Juan Mountains, Colorado, as indicated by potassium–argon dating. Geol. Soc. Am. Bull. 81, 2329–2352.

Lipman, P.W., Dungan, M., Bachmann, O., 1997. Comagmatic granophyric granite in the Fish Canyon Tuff, Colorado: implications for magma-chamber processes during a large ash-flow eruption. Geology 25, 915–918.

Mason, B.G., Pyle, D.M., Oppenheimer, C., 2004. The size and frequency of the largest explosive eruptions on Earth. Bull. Volcanol. 66, 735–748.

Matchan, E.L., Phillips, D., 2014. High-precision multi-collector ^{40}Ar/^{39}Ar dating of young basalts: Mt Rouse volcano (SE Australia) revisited. Quat. Geochron. 22, 57–64.

Mitchell, J.G., 1968. The argon-40/argon-39 method for potassium–argon age determination. Geochim. Cosmochim. Acta 32, 781–790.

Naeser, C.W., Zimmermann, R.A., Cebula, G.T., 1981. Fission track dating of apatite and zircon: an interlaboratory comparison. Nucl. Tracks 5, 65–72.

Oberli, F., Fischer, H., Meier, M., 1990. High-resolution ^{238}U–^{206}Pb zircon dating of Tertiary bentonites and Fish Canyon Tuff: a test for age "concordance" by single crystal analysis. In: 7th Internat. Conf. on Geochronology Cosmochronology and Isotope Geochemistry. In: Geol. Soc. Aust. Abstr., vol. 27, p. 74.

Oberli, F., Bachmann, O., Meier, M., Dungan, M.A., 2002. The Fish Canyon Tuff: Ar–Ar versus U–Pb age discrepancy reassessed. Geochim. Cosmochim. Acta 66 Supp, A565.

Paces, J., Miller, J., 1993. Precise U–Pb ages of Duluth Complex and related mafic intrusions, northeastern Minnesota: geochronological insights to physical, petrogenetic, paleomagnetic, and tectonomagmatic processes associated with the 1.1 Ga Midcontinent Rift System Source. J. Geophys. Res. 98, 13997–14018.

Phillips, D., Matchan, E.L., 2013. Ultra-high precision $^{40}Ar/^{39}Ar$ ages for Fish Canyon Tuff and Alder Creek Rhyolite sanidine: new dating standards required? Geochim. Cosmochim. Acta 121, 229–239.

Quidelleur, X., Grove, M., Lovera, O.M., Harrison, T.M., Yin, A., Ryerson, F.J., 1997. The thermal evolution and slip history of the Renbu Zedong Thrust, southeastern Tibet. J. Geophys. Res. 102, 2659–2679.

Reid, M.R., Coath, C.D., Harrison, T.M., McKeegan, K.D., 1997. Ion microprobe dating of young zircons reveals prolonged residence times for the youngest rhyolites associated with Long Valley caldera. Earth Planet. Sci. Lett. 150, 27–35.

Reiners, P.W., Farley, K.A., 1999. Helium diffusion and (U–Th)/He thermochronometry of titanite. Geochim. Cosmochim. Acta 63, 3845–3859.

Reiners, P.W., Farley, K.A., Hickes, H.J., 2002. He diffusion and (U–Th)/He thermochronometry of zircon: initial results from Fish Canyon Tuff and Gold Butte. Tectonophysics 349, 297–308.

Reiners, P.W., Thomson, S.N., McPhillips, D., Donelick, R.A., 2007. Wildfire thermochronology and the fate and transport of apatite in hillslope and fluvial environments. J. Geophys. Res., Earth Surf. 112, F4. http://dx.doi.org/10.1029/2007JF000759.

Renne, P.R., 1998. Intercalibration of standards and other sources of error in Ar/Ar dating. Geol. Assoc. Can. Min. Assoc. Can. Abstr. 23, A154.

Renne, P.R., Deino, A.L., Walter, R.C., Turrin, B.D., Swisher, C.C., Becker, T.A., Curtis, G.A., Sharp, W.D., Jaouni, A.-R., 1994. Intercalibration of astronomical and radioisotopic time. Geology 22, 783–786.

Renne, P.R., Swisher, C.C., Deino, A.L., Karner, D.B., Owens, T.L., DePaolo, D.J., 1998. Intercalibration of standards, absolute ages and uncertainties in $^{40}Ar/^{39}Ar$ dating. Chem. Geol. 145, 117–152.

Renne, P.R., Mundil, R., Balco, G., Min, K., Ludwig, K.R., 2010. Joint determination of ^{40}K decay constants and $^{40}Ar^*/^{40}K$ for the Fish Canyon sanidine standard, and improved accuracy for $^{40}Ar/^{39}Ar$ geochronology. Geochim. Cosmochim. Acta 74, 5349–5367.

Renne, P.R., Balco, G., Ludwig, K.R., Mundil, R., Min, K., 2011. Response to the comment by W.H. Schwarz et al. on "Joint determination of ^{40}K decay constants and $^{40}Ar^*/^{40}K$ for the Fish Canyon sanidine standard, and improved accuracy for $^{40}Ar/^{39}Ar$ geochronology". Geochim. Cosmochim. Acta 75, 5097–5100.

Schmitz, M.D., Bowring, S.A., 2001. U–Pb zircon and titanite systematics of the Fish Canyon Tuff: an assessment of high precision U–Pb geochronology and its application to young volcanic rocks. Geochim. Cosmochim. Acta 65, 2571–2587.

Schmitz, M.D., Bowring, S.A., Ludwig, K.R., Renne, P.R., 2003. Comment on "Precise K–Ar, ^{40}Ar–^{39}Ar, Rb–Sr and U–Pb mineral ages from the 27.5 Ma Fish Canyon Tuff reference standard" by M.A. Lanphere and H. Baadsgaard. Chem. Geol. 199, 277–280.

Schwarz, W.H., Kossert, K., Trieloff, M., Hopp, J., 2010. Comment on the "Joint determination of ^{40}K decay constants and $^{40}Ar^*/^{40}K$ for the Fish Canyon sanidine standard, and improved accuracy for $^{40}Ar/^{39}Ar$ geochronology" by Paul R. Renne et al. Geochim. Cosmochim. Acta 75, 5094–5096.

Spell, T.L., McDougall, I., 2003. Characterization and calibration of $^{40}Ar/^{39}Ar$ dating standards. Chem. Geol. 198, 189–211.

Steiger, R.H., Jäger, E., 1977. Subcommission on geochronology: convention on the use of decay constants in geo- and cosmochronology. Earth Planet. Sci. Lett. 36, 359–362.

Steven, T.A., Mehnert, H.H., Obradovich, J.D., 1967. Age of volcanic activity in the San Juan Mountains, Colorado. U.S. Geol. Surv. Prof. Pap. 575-D, 47–55.

Steven, T.A., Lipman, P.W., Hail, W.J., Barker, F., Luedke, R.G., 1974. 1:250 000 geologic map of the Durango Quadrangle, southwestern Colorado. U.S. Geol. Surv. Misc. Investig. Ser. Map I-764.

Tagami, T., Farley, K.A., Stockli, D.F., 2003. (U–Th)/He geochronology of single zircon grains of known Tertiary eruption age. Earth Planet. Sci. Lett. 207, 57–67.

Vermeesch, P., 2009. RadialPlotter: a Java application for fission track, luminescence and other radial plots. Radiat. Meas. 44, 409–410.

Whitney, J.A., Stormer, J.C., 1985. Mineralogy, petrology and magmatic conditions from the Fish Canyon Tuff, Colorado. J. Petrol. 26, 726–762.

Wotzlaw, J.-F., Schaltegger, U., Frick, D.A., Dungan, M.A., Gerdes, A., Günther, D., 2013. Tracking the evolution of large-volume silicic magma reservoirs from assembly to supereruption. Geology 41, 867–870.

Yoshioka, T., Tsuruta, T., Iwano, H., Danhara, T., 2005. Spontaneous fission decay constant of 238U determined by SSNTD method using CR-39 and DAP plates. Nucl. Instrum. Methods 555, 386–395.